Improving the energy efficiency of CO_2 conversion in nonequilibrium plasmas through pulsing

Improving the Energy Efficiency of CO_2 Conversion in Non-equilibrium Plasmas Through Pulsing

Vincent Vermeiren and Annemie Bogaerts*

Department of Chemistry, Research group PLASMANT, University of Antwerp, Universiteitsplein 1, 2610 Antwerp, Belgium

E-mail: annemie.bogaerts@uantwerpen.be

Abstract

Non-equilibrium plasmas offer a pathway for energy efficient CO_2 conversion through vibrationally induced dissociation. However, the efficiency of this pathway is limited by a rise in gas temperature, which increases vibrational-translational (VT) relaxation and quenches the vibrational levels. Therefore, we investigate here the effect of plasma pulsing on the VT non-equilibrium and on the CO_2 conversion, by means of a 0D chemical kinetics model, with self-consistent gas temperature calculation. Specifically, we show that higher energy efficiencies can be reached by correctly tuning the plasma pulse and interpulse times. The ideal plasma pulse time corresponds to the time needed to reach the highest vibrational temperature. In addition, the highest energy efficiencies are obtained with long interpulse times, i.e. ≥ 0.1 s, in which the gas temperature can entirely drop to room temperature. Furthermore, additional cooling of the reactor walls can give higher energy efficiencies at shorter interpulse times of 1 ms. Finally, our model shows that plasma pulsing can significantly improve the

energy efficiency at low reduced electric fields (50 and 100 Td, typical for microwave and gliding arc plasmas), and intermediate ionization degrees (5×10^{-7} and 10^{-6}).

1 Introduction

The problem of global climate change due to the emission of greenhouse gasses has accelerated the transition from fossil fuelled energy sources to renewable ones.[1] However, the intermittency of these energy sources makes their implementation challenging. Hence, there is an urgent need for more research on methods to store this excess electrical energy at peak production. Low temperature plasmas are promising for this purpose, because they can easily convert electrical energy to chemical energy. The high thermodynamic non-equilibrium between the electron temperature and gas temperature in plasma allows for endothermic reactions to take place without the need to first heat up the gas, thus lowering the energy cost with respect to pure thermal processes.[2] Current research efforts focus on the conversion of CO_2 into CO and 1/2 O_2.[3] Subsequently, CO can be combined with hydrogen as feed gas for the Fischer-Tropsch synthesis of value added chemicals, including green fuels.

The most common type of discharges for this application are microwave (MW) discharges,[4–9] gliding arc (GA) discharges[10–12] and dielectric barrier discharges (DBDs),[13–17] but atmospheric pressure glow discharges (APGDs),[18,19] corona discharges,[20,21] and ns pulsed discharges[22–24] are also being investigated. The energy efficiencies for CO_2 conversion can differ significantly among the various plasma types, which is attributed to the different dissociation pathways. DBDs are characterized by a relatively high electron temperature (ca. 2 -3 eV),[25,26] resulting in dissociation through electron impact electronic excitation,[25,27] which requires an energy of minimum 7 eV to reach a repulsive electronically excited state. In contrast, GA and MW plasmas exhibit a relatively low electron temperature (ca. 1-2 eV),[3,25,26] allowing for an efficient excitation of the asymmetric vi-

brational mode of CO_2.[25,27] These vibrationally excited molecules will then exchange vibrational energy through a mechanism called vibrational-vibrational (VV) relaxation, until the molecules reach the dissociation limit.[25] This process is called vibrational ladder climbing and requires only 5.5 eV of energy, i.e., the C=O bond dissociation energy.

However, the efficiency of the ladder climbing is limited through the loss of vibrational energy in gas heating, in a process called vibrational-translational (VT) relaxation.[2,3,25,27–29] This VT relaxation process becomes more prominent at higher gas temperature[27,28] causing even more gas heating (self-acceleration). For efficient vibrationally induced dissociation, it is therefore crucial that a strong non-equilibrium exists between the vibrational temperature and the gas temperature.[27] However, most MW and GA plasmas, especially at higher pressures and specific energy inputs (SEI), are close to thermal equilibrium.[8,11,29–31] In this case, CO_2 conversion mostly occurs through thermal dissociation, because the vibrational distribution function (VDF) follows a Boltzmann distribution, without overpopulation of the higher vibrational levels, needed for efficient dissociation.[29,30] Hence, at these conditions, the plasma does not fully make use of the potential of the vibrationally induced dissociation process.

Plasma power modulation through pulsing might be an interesting pathway to increase the vibrational-translational non-equilibrium. The main argument to indicate its potential lies in the characteristic timescales of the VV and VT processes. The timescale for VT relaxation is several orders of magnitude higher than for VV relaxation of the asymmetric mode of CO_2. By adjusting the plasma on-time accordingly, VT relaxation can thus be limited with respect to VV relaxation. Also, the characteristic timescale for VT relaxation decreases with increasing gas temperature, while that of VV relaxation increases. Given that the plasma is cooled between two consecutive pulses, the vibrational translational non-equilibrium can be enhanced in the next pulse, which has again a beneficial effect on the characteristic timescales of VV and VT relaxation. These timescales are discussed in more detail in section 2 of the SI.

The effect of power modulation in CO_2 plasmas has predominantly been studied in DBDs.[15,25,32,33] While it is shown that the energy efficiency increases in the so-called 'burst mode' with respect to the usual AC mode,[32] the electron temperature in a DBD is too high for efficient use of vibrationally induced dissociation.[25] Pulsed MW plasma experiments have been performed in CO_2 flows with N_2 admixtures by Silva et al.,[4] at pressures of 1.33-13.33 mbar. The authors measured the vibrational temperature of the electronically excited states of the N_2 admixture through optical emission spectroscopy. They showed that this vibrational temperature was much higher than the gas temperature, leading them to conclude that CO_2 dissociation could take place through vibrationally excited CO_2 levels. The work was continued by Britun et al.,[9] who measured the conversions and energy efficiencies at different pulse repetition rates, reaching a maximum conversion of 23 % and energy efficiency of 33 %, at a pressure of 9.7 mbar, a pulse repetition rate of 0.5 kHz, a flow rate of 2.7 slm, and a duty cycle of 50%. The conversion and energy efficiency dropped upon rising pulse repetition rate, while keeping all the other conditions fixed. Furthermore, with lower pulse repetition rate, when the energy efficiency was the highest, the vibrational temperature reached a maximum value, and dropped upon rising pulse repetition rate. However, a similar trend was also observed for the gas temperature. Power modulation of CO_2 MW plasmas was also studied by van den Bekerom et al.[31] The energy efficiency increased with lower duty cycle and higher peak power, but the time in between the pulses was too short to allow for significant gas cooling, resulting in a close-to-thermal equilibrium, in which the vibrationally induced dissociation does not play an important role.

Although a strong effect of power modulation on the conversion and energy efficiency has been demonstrated experimentally, more insight is needed to determine its full potential. Moreover, it is not clear from these experiments that vibrational excitation is the key to increased efficiency. Therefore, in this work, we will examine the effect of different plasma on and off times on the conversion, energy efficiency, and the underlying

mechanisms of CO_2 conversion.

2 Model Description

2.1 Plasma Model

We use the code ZDPlasKin[34] to develop a zero-dimensional (0D) chemical kinetics model, describing the temporal evolution of the different species densities, by

$$\frac{dn_s}{dt} = \sum_j R_j[a_{sj}^R - a_{sj}^L] = \sum_j (k_j \prod_l n_l)[a_{sj}^R - a_{sj}^L] \quad (1)$$

in which index j refers to reaction j and index l refers to the different reactants of reaction j. a_{sj}^R and a_{sj}^L are the right- and left-hand side stoichiometric coefficients of species s, respectively. k_j is the reaction rate coefficient of reaction j, with $R_j = k_j \prod_l n_l$ the reaction rate. The ZDPlasKin framework couples a chemical kinetics solver to the Boltzmann solver BOLSIG+,[35] which calculates the electron kinetics. In this Boltzmann solver, the electron energy distribution function (EEDF) is calculated using a set of cross sections (Table S1 in the Supporting Information; SI), including superelastic collisions. The EEDF is regularly updated during the calculations, upon changes of the gas temperature, the electron density, the reduced electric field, or the density of species reacting with electrons. The EEDF and the various cross sections are used to calculate the energy dependent rate coefficients of the electron impact reactions.

In this work, we will describe the time evolution of a volume element moving through a plasma reactor. The model starts at $t = 0$ with pure CO_2 and a Boltzmann vibrational distribution function (VDF). During the pulses, the plasma is ignited by applying a certain DC reduced electric field E/N (with E the electric field and N the gas number density) and by fixing the electron density (n_e) to a value determined by the ionization degree (d_i) $n_e = N d_i$. During the interpulses, and in the afterglow, the electron density and

reduced electric field are set to zero. The power density applied to sustain a plasma at these conditions is calculated using Joule's law: $P_{dep} = \sigma E^2 = \sigma N^2 (E/N)^2$, with σ the conductivity, which is given by $\sigma = e n_e \mu_e$. The electron mobility μ_e is obtained from the Boltzmann solver, and e is the elementary charge.

In this work, we chose a fixed pressure of 100 mbar, as it is representative for MW experiments yielding good energy efficiency.[6,8,36] During the plasma pulses, we fix the values of the reduced electric field and ionization degree to those that are typical in MW and GA plasmas, 50 Td and 10^{-6}.[3,8,37] These values show the clearest potential of power modulation. The electron density thus reaches values of 2×10^{12} cm^{-3} and scales linearly with the ionization degree. For DBD plasmas, the ionization degree can reach values up to 10^{-4}.,[38] and they generally operate at reduced electric fields above 100 Td.[3,39] Therefore, later in this paper, we will vary the ionization degree, and reduced electric field, to study their effect on the potential of pulsed power as well.

The plasma power will either activate the gas, which can lead to dissociation of CO_2 into CO and $\frac{1}{2}O_2$, or heat the gas. Given that the pressure stays constant inside the discharge, this will lead to gas expansion, and thus changing gas density. This effect is taken into account by the introduction of a variable $\beta(t)$, the gas expansion factor, which is defined by

$$\beta(t) = \frac{M(t=0) T_g(t=0)}{M(t) T_g(t)} \tag{2}$$

with M the total number of particles, and T_g the gas temperature. $\beta(t)$ is initially equal to 1, and decreases when the gas expands. For example, if the gas temperature doubles from 300 K to 600 K, the volume doubles and $\beta = 0.5$. Similarly, when all CO_2 would dissociate without an increase in temperature, then $\beta = \frac{2}{3}$, since the initial number of particles M(0) increases to $\frac{3}{2}$M(0), which will expand the gas in order to keep the density at N_0, determined by the ideal gas law.

In this study, we apply a power deposition in a series of pulses, which will end when

the total applied power reaches a certain specific energy input (SEI). This allows us to compare more easily different cases with the same deposited energy. The SEI at $t = \Delta t$ is defined as the total energy input per CO_2 molecule at $t = 0$. This can be expressed as:

$$SEI = \frac{\int_0^{\Delta t} \frac{P_{dep}(t)}{\beta(t)} dt}{N(0)} = \int_0^{\Delta t} \left(\frac{E}{N}\right)^2 \frac{\mu_e e d_i}{\beta(t)} \left(\frac{p}{k_B T_g}\right)^2 dt \tag{3}$$

with p the pressure, and k_B the Boltzmann constant.

The goal of the simulations is to find conditions that provide maximum conversion and energy efficiency. The CO_2 conversion is calculated as

$$X(t)[\%] = \left[1 - \frac{n_{CO_2}(t)}{\beta(t) N(0)}\right] \times 100\% \tag{4}$$

where n_{CO_2} is the total number density of all CO_2 molecules (ground state, and all vibrationally and electronically excited molecules) at a given time t. The energy efficiency η is calculated using the SEI and the reaction enthalpy of CO_2 splitting ($CO_2 \rightarrow CO + \frac{1}{2}O_2$) at the inlet temperature of 300 K, i.e. ΔH^o = 2.93 eV/molec:

$$\eta[\%] = X[\%] \frac{\Delta H^o}{SEI} \tag{5}$$

where the SEI value is an input to the model.

The gas temperature is calculated self-consistently in the model, using the following equation

$$N \frac{\gamma k_B}{\gamma - 1} \frac{dT_g}{dt} = P_{el} + \sum_j R_j \Delta H_j - P_{ext} \tag{6}$$

where $\gamma = c_p/c_v$ is the ratio of specific heats, P_{el} is the gas heating power density due to elastic electron-neutral collisions, ΔH_j the heat released (or consumed) in reaction j, and P_{ext} the power loss density due to exchanges with the surroundings. The ratio of specific heat is changed depending on the concentration of the different species. We will

take this external cooling term to be[28,29]

$$P_{ext} = \frac{8(\lambda + \lambda_{add})}{R^2}(T_g - T_w) \tag{7}$$

in which λ is the gas thermal conductivity, and T_w is the wall temperature taken as 300 K. We take $\lambda(T_g) = (0.071T_g - 2.33) \times 10^{-3} W m^{-1} K^{-1}$ following.[28] More details of the procedure to obtain λ are explained in.[28] R is the radius of the reactor, which is set to 7mm.[4,9] We can add an additional thermal conductivity $\lambda_{add}[W m^{-1} K^{-1}]$ to the equation, which can be changed manually to study the effect of additional cooling on the pulsing performance. Indeed, in reality, a higher thermal conductivity can be achieved in turbulent flow regimes,[40] and this turbulent conductivity has been shown to exert a cooling effect on the plasma.[41]

Finally, we also calculate the vibrational temperature of CO_2, based on the population of the first asymmetric mode level:

$$T_v = \frac{-E_1}{ln\left(\frac{n_1}{n_0}\right)} \tag{8}$$

where E_1 is the energy of the first asymmetric mode level (3380 K), with n_1 its density, and n_0 the ground state density of CO_2.

2.2 Chemistry Set

The chemistry set used in this work is similar to the one used in our previous work.[27,42] It is the result of a chemistry reduction[43] of the original full set,[25,28,44] and of a careful analysis of the uncertainties.[42] The reduced set was justified by the fact that some species had a minor effect on the model outcome, and including them only had a negative impact on the uncertainty of the model results.[42] Furthermore, ref. 42 revealed that while the uncertainty on specific important calculation results, such as the CO_2 conversion, can reach up to 100 %, the trends predicted by the model are typically not affected by the

uncertainty on the rate coefficient data, implying that this type of modelling should focus more on trends rather than absolute values.

The species that are included in this work are listed in table 1. The set includes 4 (degenerate) symmetric mode vibrational levels, and 21 asymmetric vibrational mode levels up to the dissociation limit. We justify taking a limited number of symmetric levels into account with the fact that the asymmetric vibrational mode levels are predominantly excited at electron temperatures of 1-3 eV,[45] and they experience a very fast energy exchange.[46] In addition, the relaxation rate constants of the asymmetric vibrational mode levels are much lower than those of the symmetric levels.[46] Hence, the asymmetric mode levels are more important for CO_2 dissociation. In reality, many additional, and possibly closely spaced, vibrational levels can exist due to mode mixing. Including them all in the model would be computationally unfeasible. However, we expect that these closely spaced vibrational levels, which become denser at higher energy, would not lead to a faster vibrational buildup, given that the rate constants for multi-quantum transitions are more than two orders of magnitude lower than those of single quantum transitions,[46] and a lot of these low energy transitions would be multi-quantum. Nonetheless, some vibrational energy could indeed go into the symmetric mode levels, either by VV relaxation or by electron impact vibrational excitation. Given the higher vibrational relaxation rate constants for these mode levels, this could result in a higher overall contribution from VT relaxation leading to less vibrational induced dissociation. In our work, this higher contribution from VT relaxation could shorten the ideal plasma pulse time. However, the message that is presented would still be the same. We plan to study the effect of adding additional symmetric vibrational levels in future work.

For CO, we take into account 10 levels, which is up till the dissociation energy of CO_2. For O_2, only 4 levels are taken into account. This is justified because the CO_2 conversion in our study is relatively low, so the CO and O_2 concentrations are relatively low as well. Moreover, in previous work, 63 CO levels were included, but these extra levels did not

really affect the chemistry.[25,28,43]

The reactions taken into account are listed in the SI. Table S1 and S2 show the electron impact reactions. The rate coefficients of the reactions in Table S1 are derived from cross section sets, taken from the LXcat database,[47] and used as input for the Boltzmann solver. The rate coefficients of the reactions in Table S2 are described by analytical expressions.

Given that the cross sections for vibrational excitation are usually only known for reactions starting from ground state CO_2 to the lower vibrational levels, the remaining cross sections for vibrational excitation between other levels are calculated using the Fridman approximation:[2]

$$\sigma_{nm}(\epsilon) = \frac{exp(\alpha(m-n-1))}{1+\beta n}\sigma_{01}(\epsilon + E_{01} - E_{nm}) \tag{9}$$

in which $E_{01} = E_1 - E_0$ and $E_{nm} = E_m - E_n$ are the energy differences between vibrational states 1 and 0 and states m and n, respectively, ϵ is the electron energy, and the parameters $\alpha = 0.5$ and $\beta = 0$. The scaling for the other electron impact reactions involving vibrationally excited CO_2 molecules, i.e. dissociation, ionization, and electronic excitation, is explained in more detail in reference.[25]

The ion-ion reactions and ion- neutral reactions are shown in Table S3. Table S4 lists the neutral reactions, for which the rate coefficients are given in the form of Arrhenius expressions. Since the vibrational energy can be used to overcome the activation energy barrier, the rate coefficients are scaled according to the Fridman-Macheret approximative α model.[2,27] Finally, the neutral reactions involving vibrational energy transfer through VT and VV relaxation between different molecules are presented in Table S5. These reactions are scaled using the Schwartz-Slawsky-Herzfeld (SSH) theory;[48] for more information, see.[25,44]

Table 1: Species described in the model.

Neutral ground state species
CO_2, CO, O_2, O, C

Charged species
CO_2^+, CO^+, CO_4^+, O^-, O_2^-, CO_3^-, CO_4^-, e^-

Excited states	Associated energy [eV]	State[a]
$O_2[v_{1-4}]$	Anharmonic oscillator	
$CO[v_{1-10}]$	Anharmonic oscillator	
$CO_2[v_{1-21}]$	Anharmonic oscillator	(00n)
$CO_2[v_a]$	0.083	(010)
$CO_2[v_b]$	0.167	(020) + (100)
$CO_2[v_c]$	0.252	(030) + (110)
$CO_2[v_d]$	0.339	(040) + (120) + (200)
$CO_2[e_1]$	10.5	$(^1\Sigma_u^+)$ + $(^3\Pi_u)$ + $(^1\Pi_u)$
$O_2[e_1]$	0.98	$(a^1\Delta_g)$
$O_2[e_2]$	1.6	$(b^1\Sigma_g^+)$
$O_2[e_3]$	4.5	$(A^3\Sigma_u^+)$ + $(C^3\Delta_u)$ + $(c^1\Sigma_u^-)$
$O_2[e_4]$	9.7	radiative levels
$O_2[e_5]$	14.7	radiative levels
$CO[e_1]$	6.22	$(a^3\Pi_r)$
$CO[e_2]$	6.8	$(a'^3\Sigma^+)$
$CO[e_3]$	7.9	$(A^1\Pi)$
$CO[e_4]$	10.4	$(b^3\Sigma^+)$
$CO[e_5]$	10.6	$(C^1\Sigma^+)$ + $(E^1\Pi)$
$CO[e_6]$	13.5	$(d^3\Delta_i)$ + $(e^3\Sigma^-)$

[a] CO_2 electronic states designation from Grofulović et al.,[49] O_2 and CO electronic states notation from Itikawa.[50]

2.3 Characteristic Time Scales of VV and VT Relaxation and Electron Impact Vibrational Excitation

In low temperature plasmas, the vibrational energy can be used to overcome the activation energy barrier of two main dissociation reactions (i.e. CO_2 + M $\rightarrow$ CO + O + M, and CO_2 + O $\rightarrow$ CO + O_2). Given the high activation energy barriers (E_a) of both reactions (i.e. E_a = 4.55 eV and E_a = 1.44 eV, respectively), the dissociation goes through the higher vibrational levels when the gas temperature is low.[27,29] In order to get high overpopulation, electron impact vibrational excitation and VV relaxation need to occur faster than VT relaxation. In figure 1, we plot the characteristic time scales for the following reactions as a function of gas temperature, in the range of interest for typical plasmas used for CO_2 conversion, and at a pressure of 100 mbar:

- e^- + CO_2 $\rightarrow$ e^- + CO_2(V1), as characteristic electron impact vibrational exciation (eV)
- CO_2 + CO_2(V1) $\rightarrow$ CO_2 + CO_2, as characteristic VT relaxation
- CO_2 + CO_2(V1) $\rightarrow$ CO_2(V1) + CO_2, as characteristic VV relaxation

The characteristic time scales for these reactions are defined as $\tau_{eV} = (n_e k_{0\rightarrow1}^{eV})^{-1}$, $\tau_{VT} = (n_{CO_2} k_{1\rightarrow0})^{-1}$, and $\tau_{VV} = (n_{CO_2} k_{1\rightarrow0}^{0\rightarrow1})^{-1}$, with $k_{0\rightarrow1}^{eV}$, $k_{1\rightarrow0}$, and $k_{1\rightarrow0}^{0\rightarrow1}$, the rate constants for eV, VT and VV processes, respectively, and with n_e, and n_{CO_2} the electron and CO_2 number densities, respectively. The rate constants for VV and VT relaxation are taken form table S5, while the electron impact vibrational excitation rate constant is calculated based upon the cross section and a Maxwellian EEDF, with average electron energy of a CO_2 plasma at a reduced electric field of 50 Td, namely 0.9 eV.[27] We plot the eV characteristic time scale not only at an ionization degree of 10^{-6}, but also at 10^{-5} and 10^{-7}, as this value greatly affects the characteristic time.

We want to note that the characteristic time scale of VV and VT relaxation corresponds to the relaxation time of an excited CO_2(V1), while the characteristic time scale of the electron impact reaction represents the time at which one CO_2 molecule gets excited. Given that eV takes place before VT can take place, this does not mean that if the time scale of VT relaxation is shorter than that of the electron impact excitation, no vibrationally excited molecules will exist. Also, the reaction rate of electron impact excitation will still be higher at comparable time scales, because the gas predominantly contains CO_2 ground state molecules. We therefore ask for caution in the comparison of these different times scales.

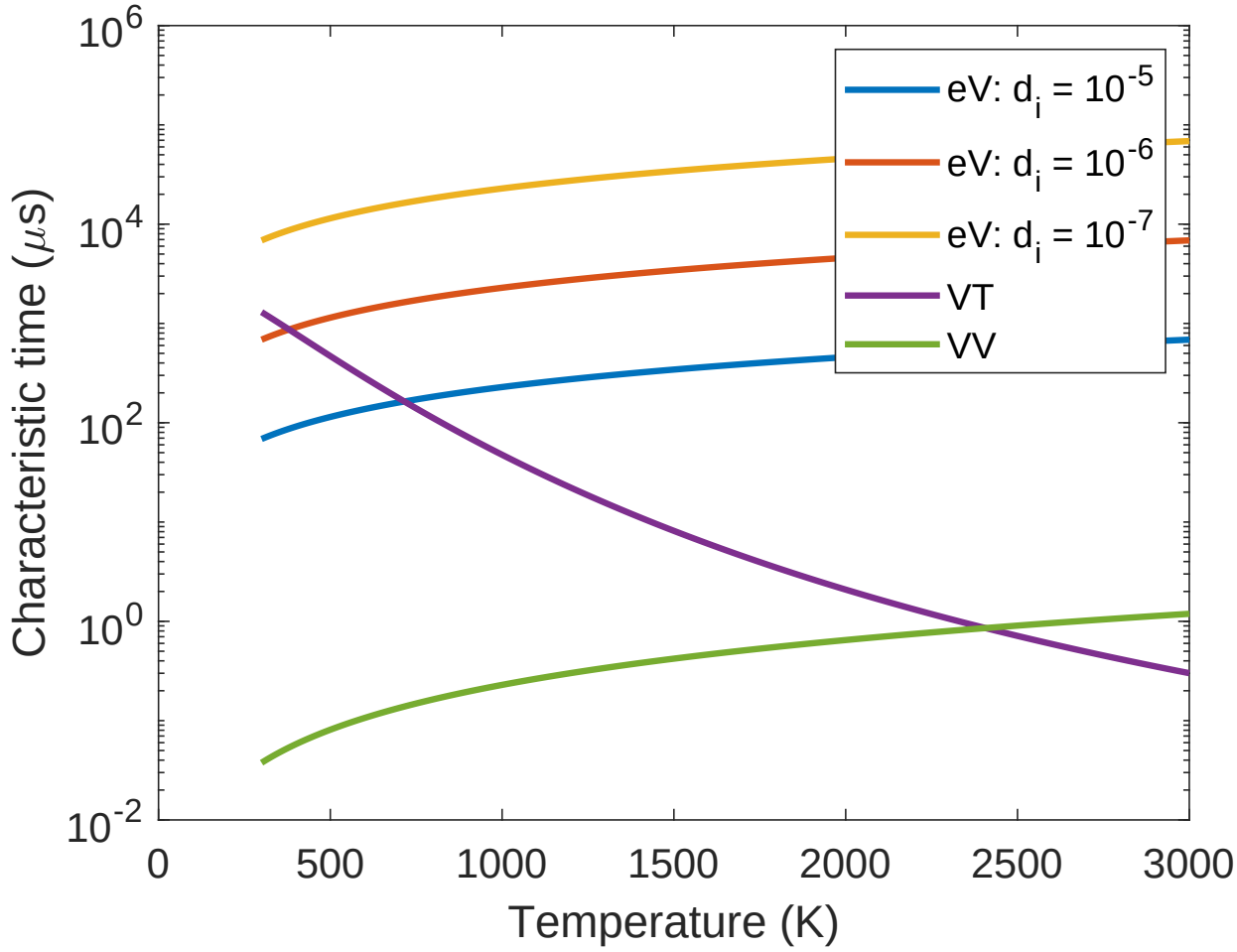

Figure 1: Characteristic time scales of electron impact vibrational excitation (eV) at three different ionization degrees (d_i) and a reduced electric field of 50 Td, and of VT and VV relaxation, as a function of gas temperature at a pressure of 100 mbar.

At 300 K, the characteristic time scale of VT relaxation (1.3 ms) is comparable to that of the electron impact vibrational excitation at $d_i = 10^{-6}$ (0.7 ms), while VV relaxation happens at a much shorter time scale (0.04 µs). This means that the rate of population of the higher vibrational levels, needed for energy efficient CO_2 dissociation is mainly limited by the electron impact vibrational excitation. This excitation process can be enhanced upon increasing ionization degree, which is logical, as there will be more electrons available for excitation. At a 10 times higher ionization degree (10^{-5}), the characteristic time scale of vibrational excitation decreases with the same factor 10. Similarly, an decrease in the ionization degree to 10^{-7} will increase the relaxation time.

The characteristic time scales of electron impact vibrational excitation and VV relaxation increase with gas temperature, while the characteristic time scale of VT relaxation decreases drastically, which is both detrimental for populating the higher vibrational levels, and thus for energy efficient CO_2 conversion. At temperatures above 2400 K, VT relaxation becomes even faster than VV relaxation. We want to note that the characteristic time scale of electron impact vibrational excitation changes with gas temperature, simply because the ionization degree is fixed and the gas density changes with gas temperature. For a constant electron density and electron temperature, the time scale would not change with gas temperature. To maximize the effect of vibrationally induced dissociation, the gas temperature thus needs to be close to room temperature, in combination with an as high as possible ionization degree, which is consistent with our previous model calculations.[27]

3 Results and Discussion

In section 3.1, we will investigate the effect of different plasma pulse and interpulse times on the CO_2 conversion and energy efficiency, for a plasma at a pressure of 100 mbar, a reduced electric field of 50 Td, and an ionization degree of 10^{-6}. Sections 3.2 and 3.3 will

be dedicated to the time-evolution of the vibrational and gas temperature throughout the first pulse, and after the first pulse, respectively, for different values of t_{on}. In section 3.4, the average vibrational and gas temperature for the different cases will be compared to those of a continuous plasma. Next, the vibrational distribution function (VDF) will be tracked through the first pulse, after the first pulse, and at the end of the plasma, in section 3.5. In section 3.6, we will demonstrate the evolution of the most important dissociation and recombination mechanisms for the different plasma pulse and interpulse times, which will be linked to the results in section 3.1. Section 3.7 will discuss the effect of additional cooling on the energy efficiency dependence of the interpulse time. Finally, in section 3.8, we will study the effect of the pulsing potential at different ionization degrees and reduced electric fields.

3.1 Effect of Pulsing on the Energy Efficiency and Conversion

Fig. 2 shows the CO_2 conversion (right y-axis) and energy efficiency (left y-axis) for different plasma pulse times (t_{on} = 1 µs, 10 µs, 40 µs, 60 µs, 100 µs) , and different interpulse times (t_{off} = 1 µs, 10 µs, 100 µs, 1 ms, 10 ms, 100 ms, 1 s) with an SEI of 1 eV/molec, at a reduced electric field of 50 Td and an ionization degree of 10^{-6}. The horizontal line corresponds to the conversion and energy efficiency of a continuous (non-pulsed) plasma at the same SEI. Note that the conversion and energy efficiency are linearly correlated, because the SEI is constant here (see eq. 5). Therefore, in the following we will only focus on the values of energy efficiency, but the same discussion applies to the conversion.

The results show two separate trends of conversion and energy efficiency upon increasing interpulse time. At short pulse times (t_{on} = 1 and 10 µs), the energy efficiency reaches a maximum of 5.5 % and 10 %, respectively, at short interpulse times of t_{off} = 1 µs. These values are, however, lower than the energy efficiency for a continuous plasma (i.e., 10.8 %). When the interpulse time increases, the energy efficiency drops considerably. The drop is more pronounced for t_{on} = 1 µs, for which the values of the energy

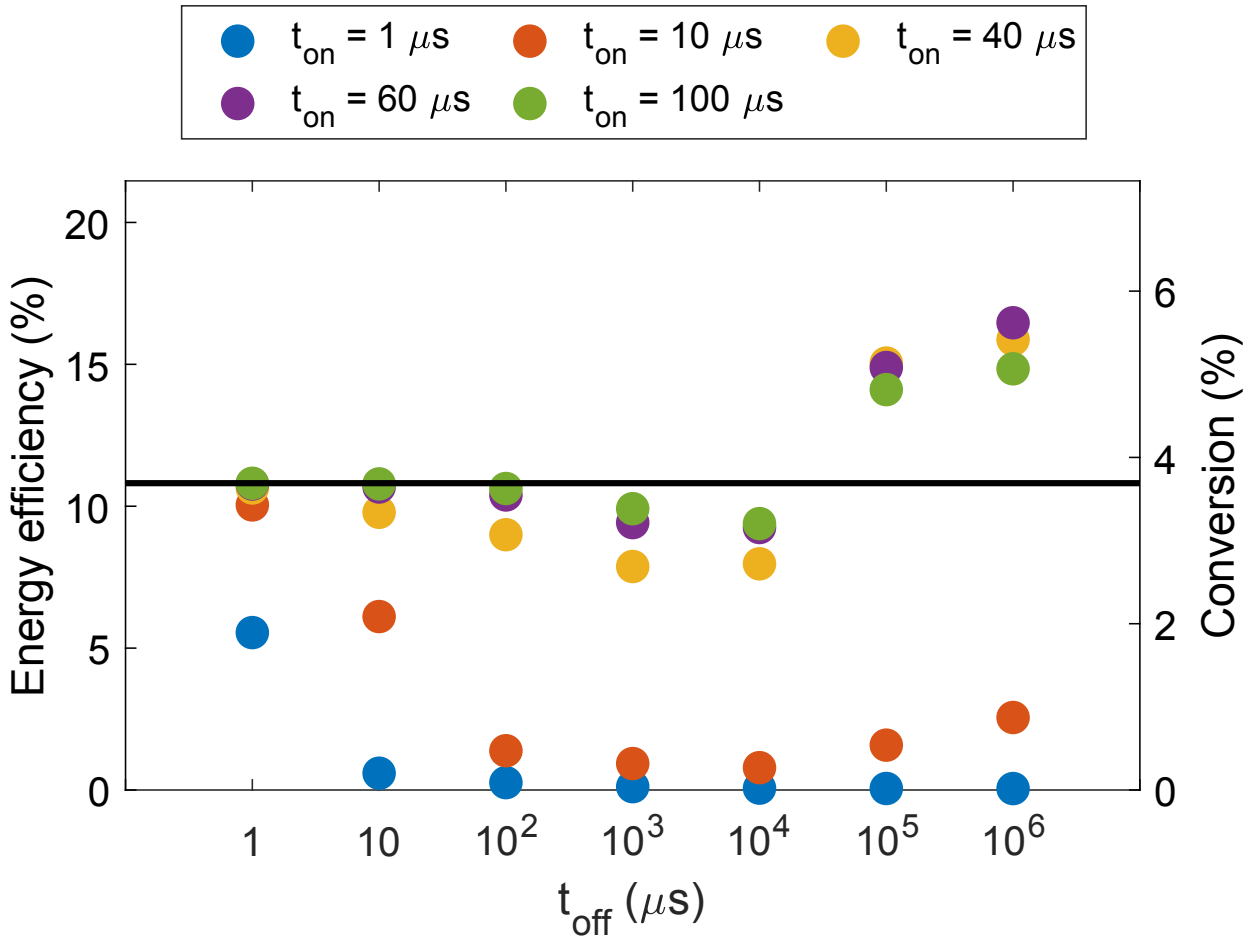

Figure 2: Energy efficiency and conversion as a function of interpulse time (t_{off}), for five different plasma on times (t_{on}), for an SEI of 1 eV/molec. The horizontal line represents the conversion and energy efficiency of a continuous plasma at the same SEI.

efficiency become negligible at interpulse times above t_{off} = 10 µs. For t_{on} = 10 µs, the energy efficiency increases again slightly at interpulse times greater than 10 ms.

For longer pulse times (t_{on} = 40, 60, and 100 µs), the energy efficiency at the shortest interpulse time (t_{off} = 1 µs) is 10.6%, 10.8% and 10.8%, respectively, hence very close to the energy efficiency of the continuous plasma. When the interpulse time increases, the energy efficiency initially decreases slightly, being most pronounced for t_{on} = 40 µs. However, when applying an interpulse time of t_{off} = 100 ms, the energy efficiency for all three pulse times becomes larger than that of the continuous plasma. A maximum energy efficiency is reached at an interpulse time of t_{off} = 1 s, yielding values of 15.9%, 16.5%, and 14.8%, for t_{on} = 40, 60, and 100 µs, respectively. Hence, a maximum relative increase of 52% in both the conversion and energy efficiency, with respect to a continuous plasma, is observed for t_{on} = 60 µs and t_{off} = 1 s. However, similarly as what was stated in section 2.2, we would like to urge the reader to focus on the trends, rather than the absolute values of the efficiencies, as they can be affected by the uncertainties on the rate coefficients. In particular, the energy efficiency was shown to greatly depend on the uncertainty on the activation energy of the reaction $CO_2 + O \rightarrow CO + O_2$.[27] If this activation energy of this reaction would be lower, the energy efficiencies would be higher.

In summary, our model reveals that a short plasma pulse and interpulse time both have a negative effect on the CO_2 conversion and energy efficiency. Indeed, the plasma pulse time and interpulse time both need to be sufficiently long ($t_{on} \geq$ 40 µs, and $t_{off} \geq$ 100 ms) to ensure a higher conversion and energy efficiency than in a continuous plasma. In the experiments conducted by Britun et al.,[9] a higher energy efficiency was also found at lower pulse repetition rates. However, a quantitative comparison of the results cannot be performed, because the experiments were conducted at a lower pressure (27 mbar) and higher specific energy input (2 eV/molec.) than in our study. In the next sections, we will explain the above trends.

3.2 Time-evolution of the Vibrational and Gas Temperature during the First Pulse

To understand the results plotted in figure 2, we first take a look at the time-evolution of the vibrational and gas temperature during the first pulse, for different plasma pulse times, i.e., t_{on} = 10, 60, and 100 µs.

Given that the build-up of the vibrational and gas temperature is the same in the first pulse for all cases, we show the gas and vibrational temperature evolution through a continuous plasma in figure 3, but we indicate the end of the pulses for the three cases by vertical dashed lines.

At the start of the plasma (t=0), the vibrational temperature immediately increases to a value of 2468 K after 10 µs, while the gas temperature does not significantly increase. This behavior is correlated with the long characteristic time scale of VT relaxation around 300 K (see figure 1), and the fact that the vibrational energy levels first need to be populated before they release their energy into heat by VT relaxation. Because of the low VT relaxation rate, the gas temperature does not significantly increase in this time frame.

After $10\mu s$, the gas temperature starts increasing monotonically until the end of the continuous plasma (i.e. when 1 eV/molec is reached). The vibrational temperature also continues to increase, but at a slower pace than before. It reaches a maximum value of 3625 K at t = 57 µs, with a corresponding gas temperature of 708 K. While the gas temperature keeps on increasing beyond that point, the vibrational temperature starts to drop until it reaches 2011 K at t = 100 µs, with a corresponding gas temperature of 1172 K. This can be correlated with the shorter characteristic time scale for VT relaxation with respect to electron impact vibrational excitation at this higher gas temperature (see figure 1). At the end of the continuous plasma (228 µs), the vibrational and gas temperature are nearly equal to each other (i.e. 1949 K vs 1862 K), indicating that there is no significant vibrational-translational non-equilibrium anymore. The evolution of the vibrational and gas temperature, described by our model, follows the same trends as in the experiments

by Klarenaar et al.[51] Note that these experiments were conducted at a lower pressure (6.7 mbar), a lower ionization degree (10^{-7}), but a similar reduced electric field (60 Td). In section 3.8, we will demonstrate, however, that the evolution of the vibrational and gas temperature is similar at lower ionization degrees.

In summary, our model reveals that a plasma pulse time of 60 µs is ideal, at the conditions investigated, because at this time the vibrational temperature reaches its maximum. For shorter plasma pulses, the vibrational temperature does not have enough time to reach this maximum value. On the other hand, at longer pulse times, VT relaxation starts to dominate, due to the high gas temperature, causing a drop in vibrational temperature. This ideal plasma pulse time of 60 µs, to reach the highest vibrational temperature, corresponds with the plasma pulse time that provides the highest conversion and energy efficiency (figure 2), clearly indicating that a high vibrational temperature is required to reach the most energy efficient CO_2 conversion.

3.3 Time-evolution of the Vibrational and Gas Temperature After the First Pulse

Figure 4 presents the vibrational and gas temperature as a function of time after the first pulse, for the three different plasma pulse times of figure 3 above, i.e., t_{on} = 10, 60, and 100 µs, as well as the afterglow of the continuous plasma. The vibrational and gas temperature are shown in full and dotted blue line, with corresponding values on the left y-axis. In addition, the gas temperature is also plotted with a red full line on a smaller scale (right y-axis) to better illustrate the finer details of its time-evolution. The calculations are performed for a long interpulse time of 1 s, but to evaluate the vibrational-translational non-equilibrium for different interpulse times, the latter are also indicated with vertical dashed lines in figure 4, with the values written in the x-axis.

The time-evolution of the vibrational temperature is very similar in all four cases. The vibrational temperature decreases fast after the first pulse, due to VT relaxation. For a

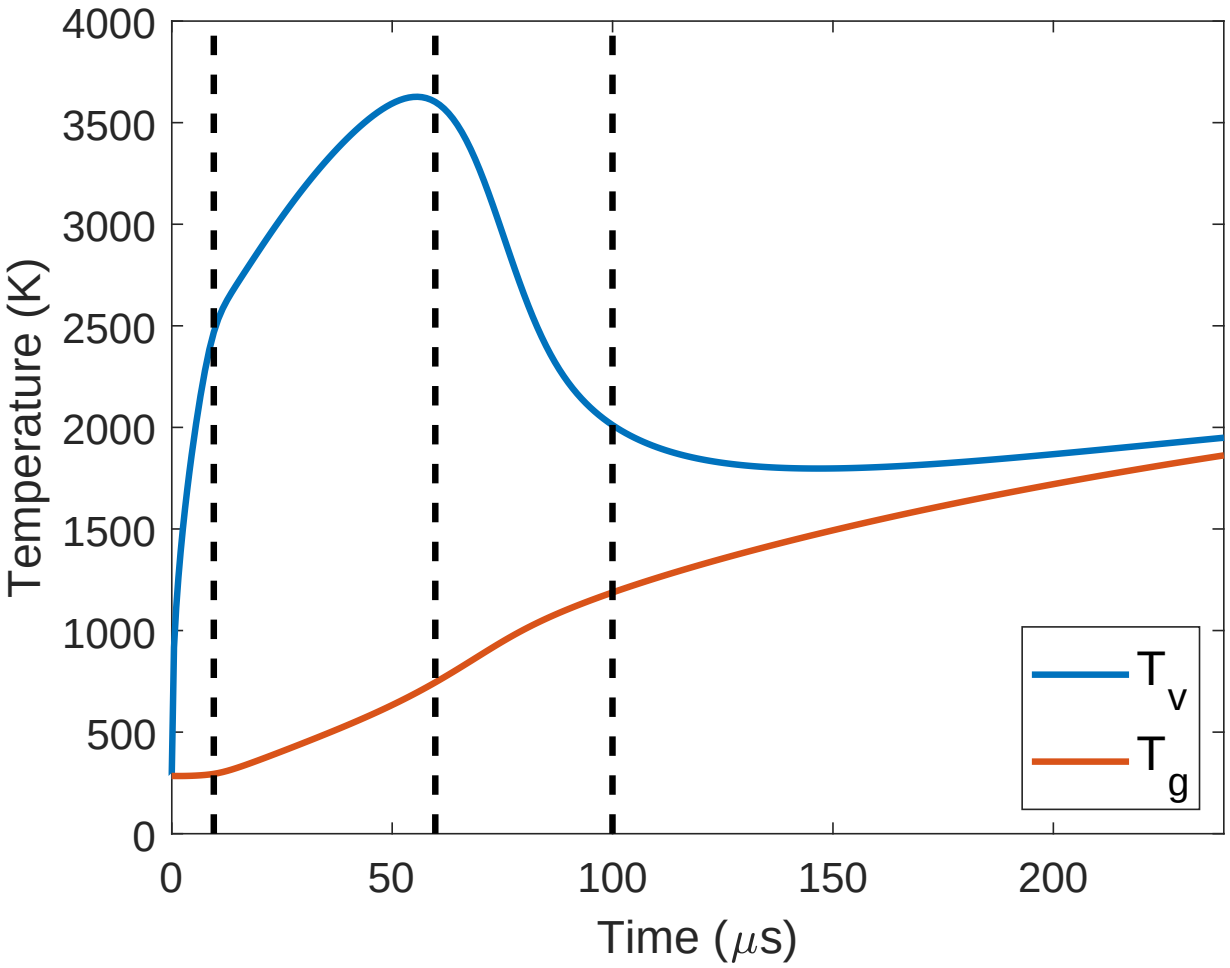

Figure 3: Time-evolution of vibrational temperature (blue line) and gas temperature (red line) during a continuous plasma. The vertical dashed lines indicate the end of the plasma pulses with t_{on} = 10, 60, and 100 µs.

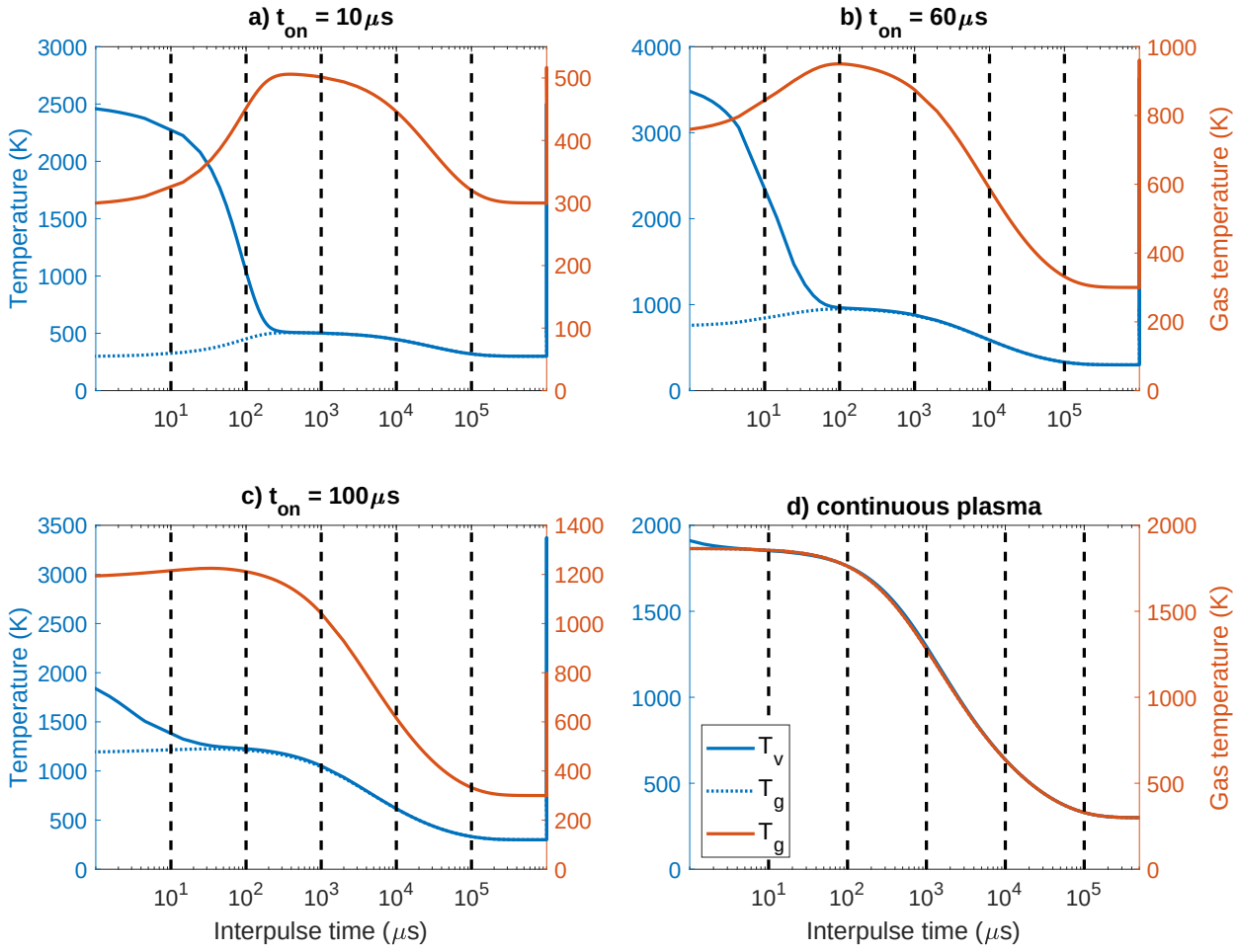

Figure 4: Time-evolution of the vibrational (full blue line - left y-axis) and gas temperature (full red line - right y-axis, as wel as blue dotted line - left y-axis, to directly compare to the vibrational temperature) after the first pulse, for the three different plasma pulses of figure 3, i.e. (a) t_{on} = 10 µs, (b) t_{on} = 60, and (c) t_{on} = 100 µs, and (d) the afterglow of a continuous plasma. To evaluate the vibrational-translation non-equilibrium for different interpulse times, the latter are indicated in the figure with vertical dashed lines.

pulse time of, t_{on} = 10 µs, a drop of 100 K is observed within 63 µs, while for the pulse times of 60 and 100 µs, a drop of 1000 K takes place within 9 µs and 1.4 ms, respectively. This temperature drop is more pronounced due to the high vibrational and gas temperature, causing more VT relaxation. For the continuous plasma, it takes 2.2 ms before the vibrational temperature has dropped by 1000 K. The reason is that the vibrational and gas temperature are in close-to thermal equilibrium at the end of the plasma, so it follows the decay of the gas temperature.

The time-evolution of the gas temperature is quite different from that of the vibrational temperature. For the pulse times of 10, 60, and 100 µs, the gas temperature first increases after the pulse. A maximum value of 506 K, 950 K, and 1225 K is found at times t = 0.38 ms, t = 0.09 ms, and t = 0.03 ms after the pulse, for t_{on}= 10 µs, 60 µs, and 100 µs, respectively. At those times, the vibrational and gas temperature differ by only 3 K, 17 K, and 31 K, respectively, and also at later times no significant non-equilibrium exists anymore between the vibrational and gas temperature. In the case of the continuous plasma, the temperature does not increase after the plasma, because the vibrational and gas temperature are already in close-to equilibrium at the end of the plasma.

After the gas temperature has reached its maximum value, it takes around 0.1 – 26 ms to drop by 100 K (i.e., 20 ms, 1.3 ms, 0.46 ms, and 0.1 ms , for t_{on} = 10 µs, 60 µs, 100 µs, and the continuous plasma, respectively). Hence, this drop is faster for the higher initial values of the gas temperature, as expected from eq. 7. These time scales are considerably longer than the characteristic time scales of the drop in vibrational temperature, when a high non-equilibrium is present (i.e., 9 – 60 µs for a drop of 1000 K; cf above). Note that the absolute numbers of these temperature and times only give an indication, and are subject to some uncertainties. More important are the trends they reveal.

In conclusion, figure 4 clearly illustrates that for the different plasma pulse times, and for interpulse times shorter than 100 µs, pulsing will further increase the gas temperature and reduce the vibrational temperature, which has a negative effect on the vibrational-

translational non-equilibrium, and hence on the vibrationally induced dissociation. At interpulse times shorter than 100 ms, the gas is still above room temperature when the next pulse would start, which should also be avoided to reach strong vibrational-translational non-equilibrium in the next pulse. Only when the interpulse time is 100 ms or 1 s, the gas is cooled down sufficiently and the vibrational and gas temperature are both at room temperature. At these interpulse times, higher conversions and energy efficiencies are indeed found with respect to a continuous plasma (cf. figure 2 above).

3.4 Average Vibrational and Gas Temperature During the Pulses

In the previous section, we saw that between the pulses, the vibrational temperature reduced, while the gas temperature increased at small interpulse times, and decreased at longer interpulse times. These gains and losses are higher for shorter plasma pulses, since a higher amount of pulses are needed to reach the same SEI. For more details, see figure S1 in section 2 of the SI, where the total vibrational and gas temperature gains and losses between the pulses are shown for different cases.

The vibrational temperature loss between the pulses needs to be compensated in subsequent pulses, which can affect the average vibrational temperature in the plasma. Figure 5 illustrates the average vibrational (blue) and gas temperature (red) during the plasma (i.e., averaged over all plasma pulse times), for different plasma pulse and interpulse times, as well as the corresponding values in the continuous plasma, depicted by the horizontal lines with similar colors. In order to compare these values of the average vibrational temperature to the energy efficiency, we include figure 6, which shows the energy efficiency (also depicted in figure 2) as a function of the average vibrational temperature, for all modelled cases.

For short plasma pulse times, i.e. $t_{on} \leq 10$ µs, the vibrational and gas temperature are closest to the values of the continuous plasma (i.e. 2292 K and 1194 K, respectively) at short interpulse times. This is consistent to figure 4, where the vibrational temperature

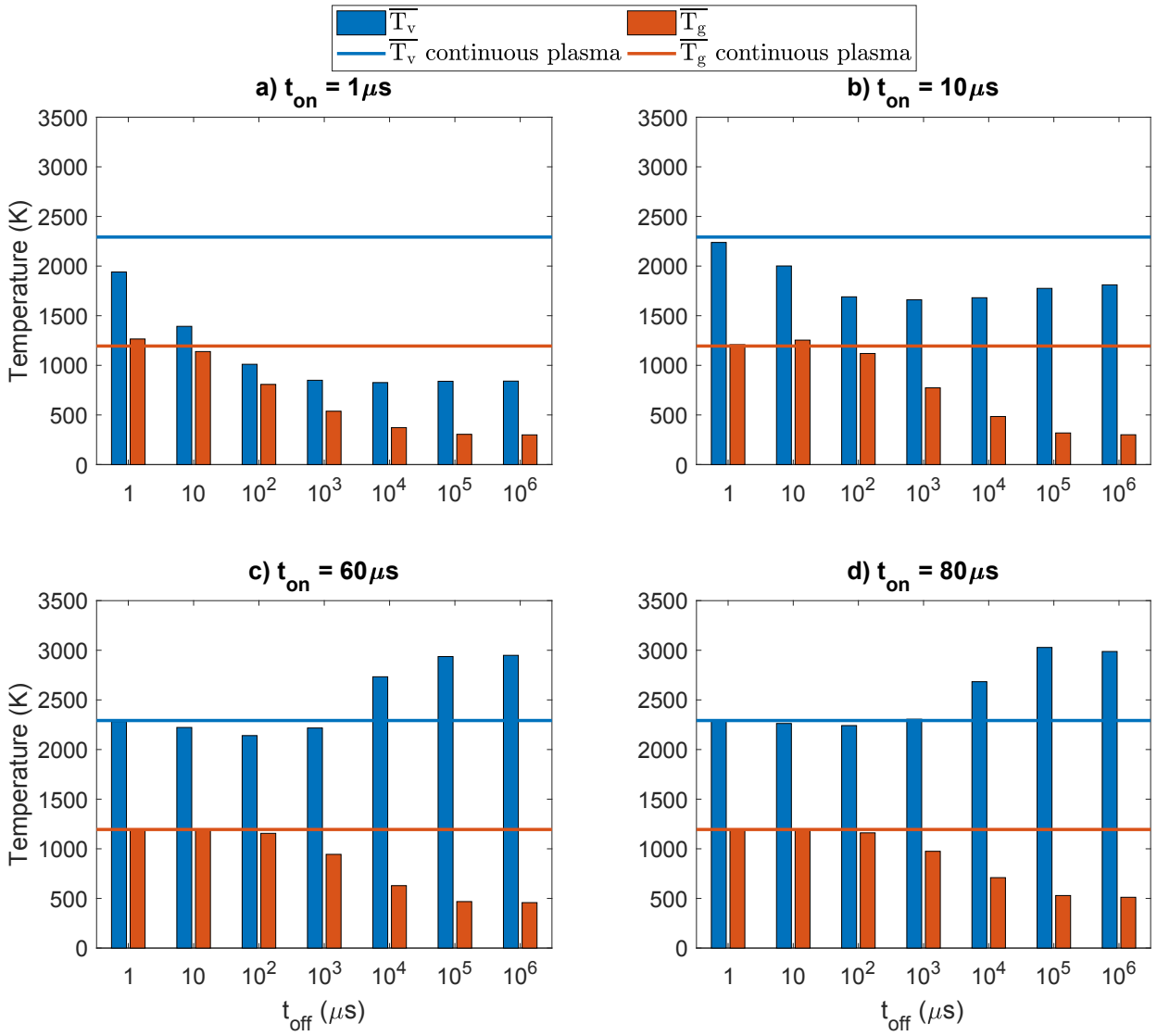

Figure 5: Average vibrational temperature (blue) and gas temperature (red), during the pulses, for different plasma pulse and interpulse times. The horizontal lines correspond to the values for the continuous plasma.

moderately decreased for short interpulses, while the gas temperature could slightly increase. Note that the rise in gas temperature after the first pulse does not lead to a higher average gas temperature, with respect to the continuous case. As the vibrational temperature is reduced, the rise in average gas temperature due to VT relaxation will be lower at the start of the next pulse. Also, later in the plasma, the gas temperature could be much higher, resulting in a stronger cooling between the pulses (see eq. 7). At interpulse

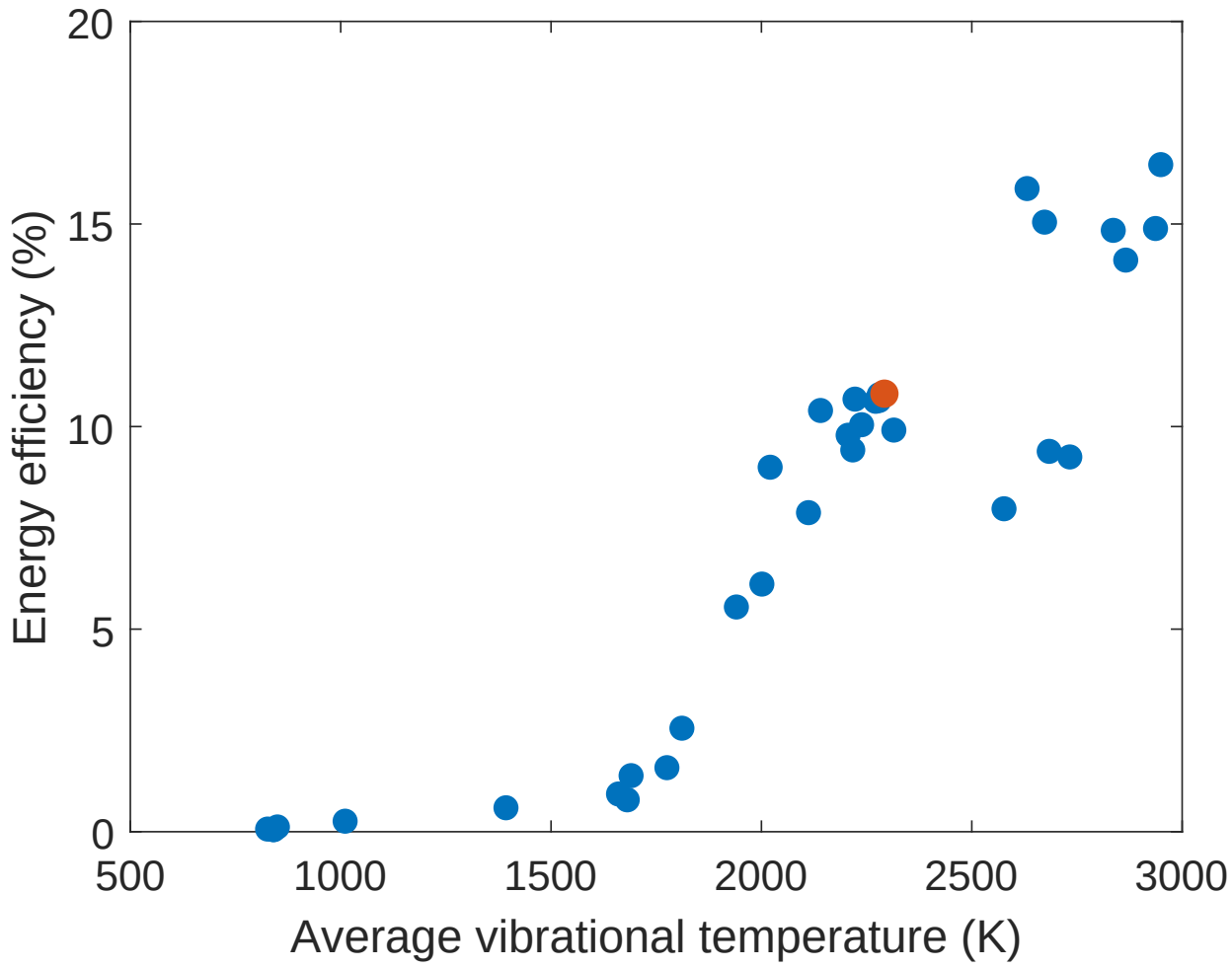

Figure 6: Energy efficiency as a function of the average vibrational temperature for different plasma pulse and interpulse times (blue), and for the continuous plasma (red).

times above 0.1 s, we see that the average gas temperature reduces to 300 K, which is most beneficial for efficient vibrationally induced dissociation.[27,29] However, the average vibrational temperature also reduces to 841 K for t_{on} = 1 µs and to 1811 K for t_{on} = 10 µs. While the low gas temperature allows for efficient vibrational excitation, the plasma pulse time is too short to reach higher values than those of the continuous plasma. For t_{on} = 10 µs, the vibrational temperature does start to increase again at $t_{off} > 10$ ms, explaining the small increase which is also noticed in figure 2.

For longer plasma pulse times (t_{on} = 60 and 100 µs), the vibrational and gas temperature are again close to the values of the continuous plasma at short interpulse times.

Again, the interpulse time is too short to allow for significant vibrational and translational changes. At $t_{off} \geq 1$ ms, the average gas temperature starts to drop until it reaches an average value of 458 K and 591 K, for t_{on} = 60 and 100 µs, respectively. This temperature drop results in an increase of the average vibrational temperature. For $t_{on} \geq 10$ ms, the average gas temperature is sufficiently reduced, which allows for the average value of the vibrational temperature to exceed the value of the continuous plasma to reach 2949 K and 2836 K at and interpulse time of 1 s for t_{on} = 60 and 100 µs, respectively. However, while the value of the vibrational temperature exceeds the value of the continuous plasma for $t_{on} \geq 10$ ms, the energy efficiency only exceeds the one from the continuous plasma for $t_{on} \geq 100$ ms (see figure 2). In order to explain this, we take a look at the VDF in the next sections.

3.5 Effect of Pulsing on the Vibrational Distribution Function (VDF)

The vibrational temperature is a strong indicator for efficient vibrationally induced dissociation. However, it is only a measure of the population of the first vibrational level (see eq. 8). As dissociation takes place from the higher vibrational levels of CO_2,[29] it is therefore also useful to study the vibrational distribution function (VDF) of the asymmetric stretch mode, which is the most important for CO_2 dissociation.[25,29] In the next sections, we will show the calculated VDFs at the end of the first pulse (for different plasma pulse times), after the first pulse (for a fixed plasma pulse time and different interpulse times), and at the end of the plasma. In each case, we will also plot the corresponding Boltzmann distribution functions at the vibrational temperature reached at these conditions, to evaluate the degree of vibrational overpopulation of the higher levels.

3.5.1 VDF at the End of the First Pulse

Similarly as what was mentioned in section 3.2 for the vibrational and gas temperature, the buildup of the VDFs during the first pulse is similar, for different plasma pulse times.

The VDFs at the end of the first pulse, for different plasma pulse times (i.e. t = 1, 10, 60, and 100 µs) are displayed in figure 7. We also added t = 80 µs, which is relevant for later discussion. The Boltzmann distributions corresponding to the vibrational temperatures, at the different pulse times, are also shown in dotted lines, to evaluate the overpopulation of the higher vibrational levels with respect to this equilibrium distribution.

At a short plasma pulse time of 1 µs, the VDF starts getting populated. While the overpopulation with respect to the equilibrium Boltzmann distribution at T_v due to the short characteristic time scale of VV relaxation at temperatures around 300 K (0.04 µs; see figure 1), the time is still too short to reach a significant population of the higher levels. This population is much more significant at a plasma pulse time of 10 µs, at which a vibrational temperature of 2468 K is reached (see also figure 3). For a plasma pulse time of 60 µs, the vibrational temperature is 3602 K. The population of the higher vibrational levels is still strong, but this is most apparent for the intermediate levels, while the highest levels (V17-V21) are somewhat depleted with respect to t = 10 µs, due to the somewhat higher gas temperature (745 K), causing more VT relaxation.

At a time of 80 µs, the gas temperature has increased to 1005 K, and VT relaxation becomes more important (cf. shorter characteristic time scale; see figure 1). It can be seen that at t = 80 µs, the vibrational temperature reduces to 2656 K. While this vibrational temperature is higher than in the case of t = 10 µs (i.e. 2468 K), the overpopulation of vibrational levels with respect to the Boltzmann distribution is considerably lower, which has a negative effect on the vibrationally induced dissociation.

For a plasma pulse time of 100 µs, the gas temperature has increased to 1187 K. While the vibrational temperature reduces to 2011 K, the higher vibrational levels get more depleted, with respect to 80 µs. However, this depletion is not as pronounced as compared to the depletion going from 60 µs to 80 µs.

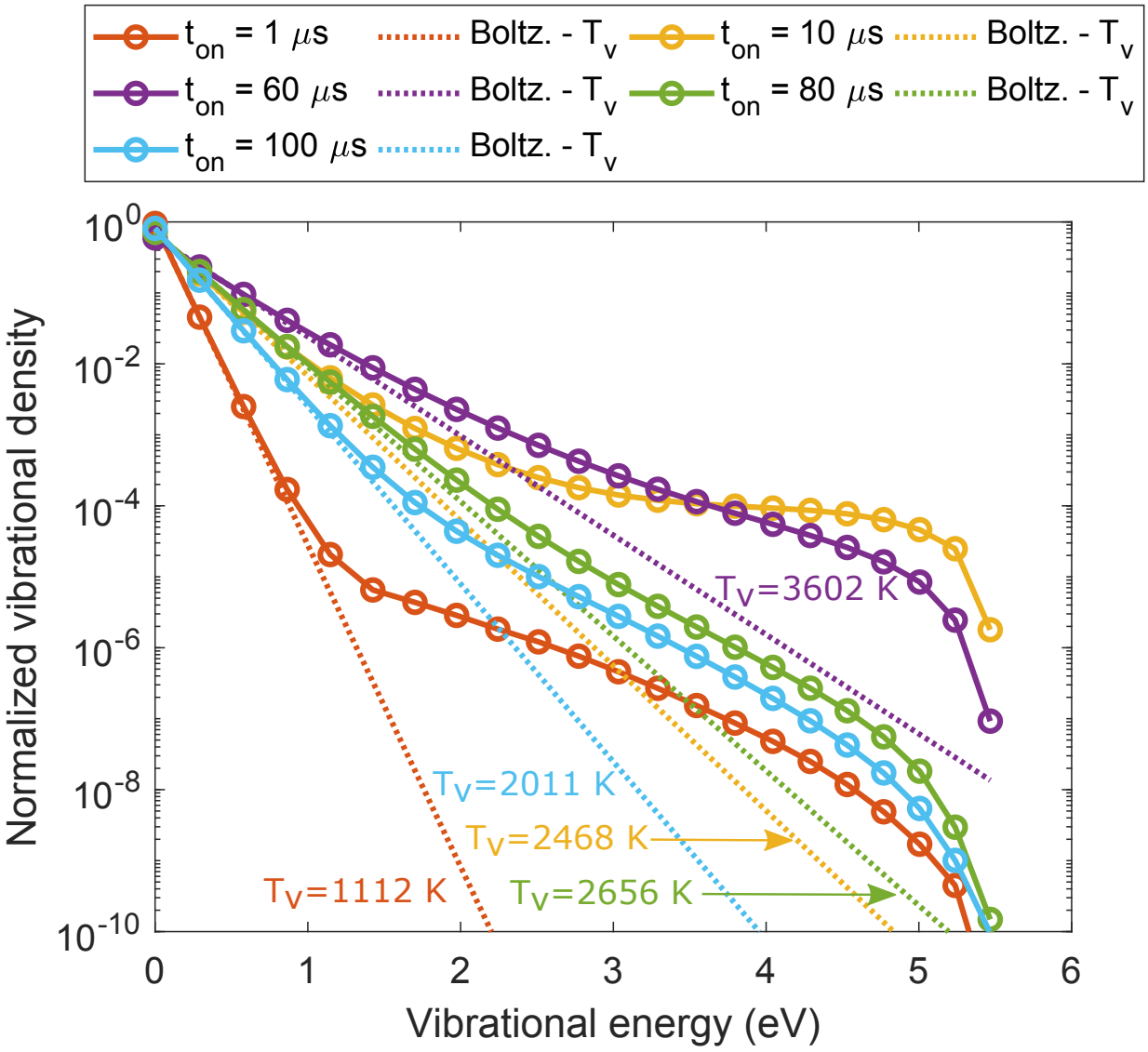

Figure 7: VDFs at the end of the first pulse, for four different plasma pulse times. The corresponding Boltzmann distribution functions at the vibrational temperature reached in these cases (cf. figure 3) are also plotted in the same color (with these vibrational temperatures indicated), to illustrate the degree of overpopulation of the higher vibrational levels with respect to this equilibrium distribution.

3.5.2 Relaxation of the VDF Between Two Pulses

In figure 8, we show the VDF at the end of the first pulse (black curve), for a plasma pulse time t_{on} = 60 µs, and before the start of a new pulse, for four different interpulse times, i.e., t_{off} = 1 µs, 10 µs, 1 ms, and 1 s. The Boltzmann plots at the corresponding vibrational temperatures are also indicated, to evaluate the degree of overpopulation of the higher levels with respect to this equilibrium distribution.

Figure 4 illustrated that the vibrational temperature quickly drops after the plasma pulse, and that a quasi-equilibrium with the gas temperature was reached at around t = 1 ms. This is also observed in the VDFs; see figure 8. At the end of the plasma pulse with t_{on} = 60 µs, the higher levels of the VDF are strongly populated (cf. also figure 7). After 1 µs , the VDF still looks very similar to the one at the end of the pulse, and only a small relaxation is noticed. After 10 µs, the higher vibrational levels are clearly less populated. While the overpopulation with respect to the Boltzmann distribution is still significant, a faster relaxation is observed for the higher vibrational levels. Similarly as in figure 4, the VDF relaxes to its Boltzmann distribution after 1 ms. For longer interpulse times, the population of the VDF still decreases, since the vibrational and gas temperature, and corresponding Boltzmann distribution decrease.

3.5.3 VDF at the End of the Plasma

Previous sections only showed the VDF and the vibrational and gas temperature during and after the first pulse, but many consecutive pulses can occur. Therefore, we plot in figure 9 the VDFs at the end of the plasma (i.e. at the end of the last full pulse in case of more than two pulses, or when the predefined SEI of 1 eV/molec. is reached), for two different plasma pulse times (i.e., 1 and 60 µs) and in each case for four different interpulse times. For comparison, the VDF in case of a continuous plasma (when the SEI of 1eV/molec. is reached) is also illustrated. In addition, in each case, the corresponding Boltzmann distributions are also plotted at the indicated vibrational temperatures, to evaluate the degree

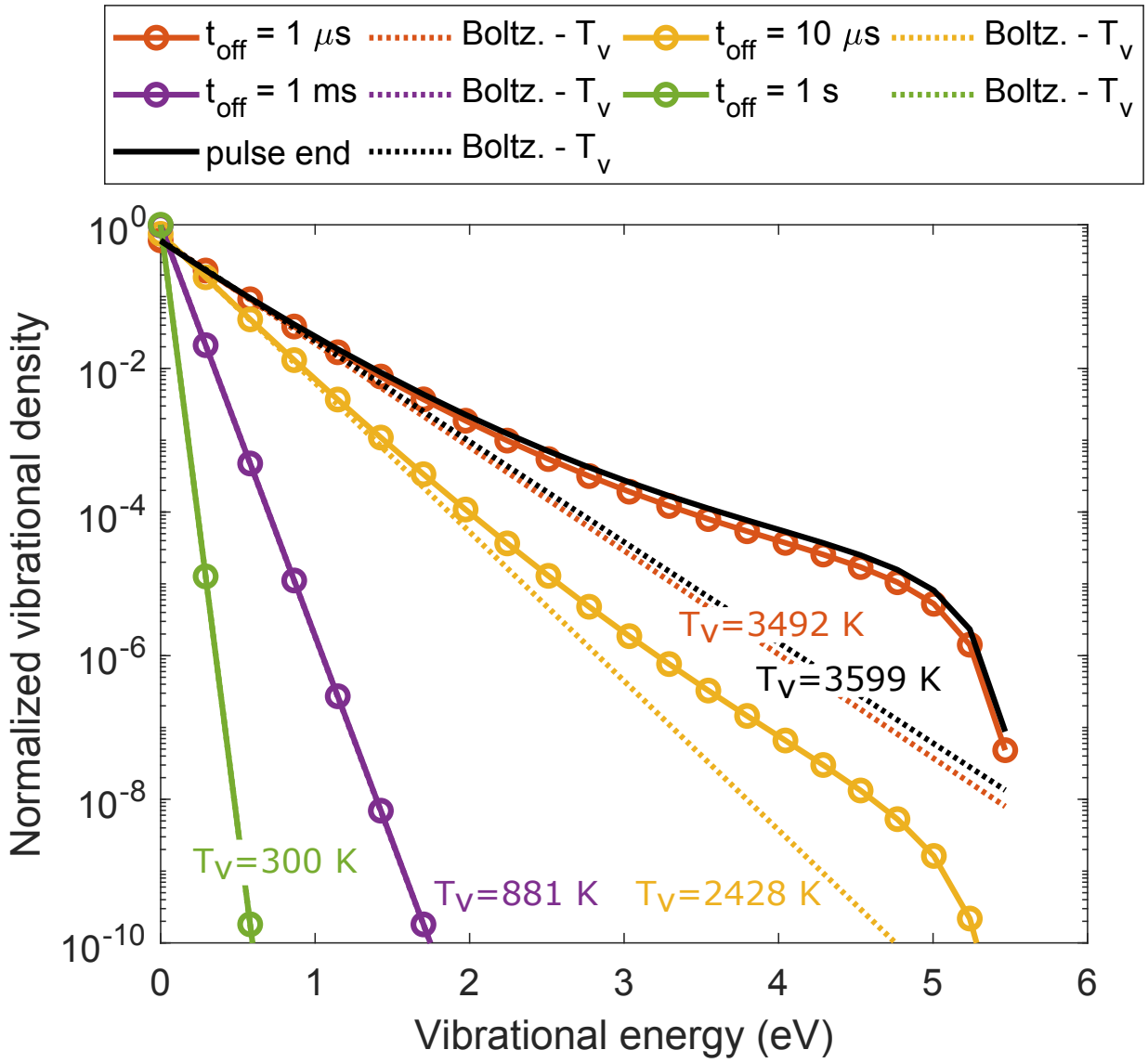

Figure 8: VDFs and the end of the first pulse, and before the start of the second pulse, for a plasma pulse time t_{on}= 60 µs, and for four different interpulse times. The corresponding equilibrium Boltzmann distribution at the vibrational temperature reached in these cases (cf. figure 4 b) are also plotted in the same color (with these vibrational temperatures indicated), to illustrate the degree of overpopulation of the higher vibrational levels with respect to this equilibrium distribution.

of overpopulation of the higher vibrational levels with respect to this equilibrium distribution. In figure S4 and S5 of the SI, we also show the VDFs at half of the plasma (i.e., when an SEI of 0.5 eV/molec is reached), for t_{on}= 1 µs and 10 µs, and the VDFs at the end of the plasma, for t_{on}= 10 µs and 100 µs, for different interpulse times.

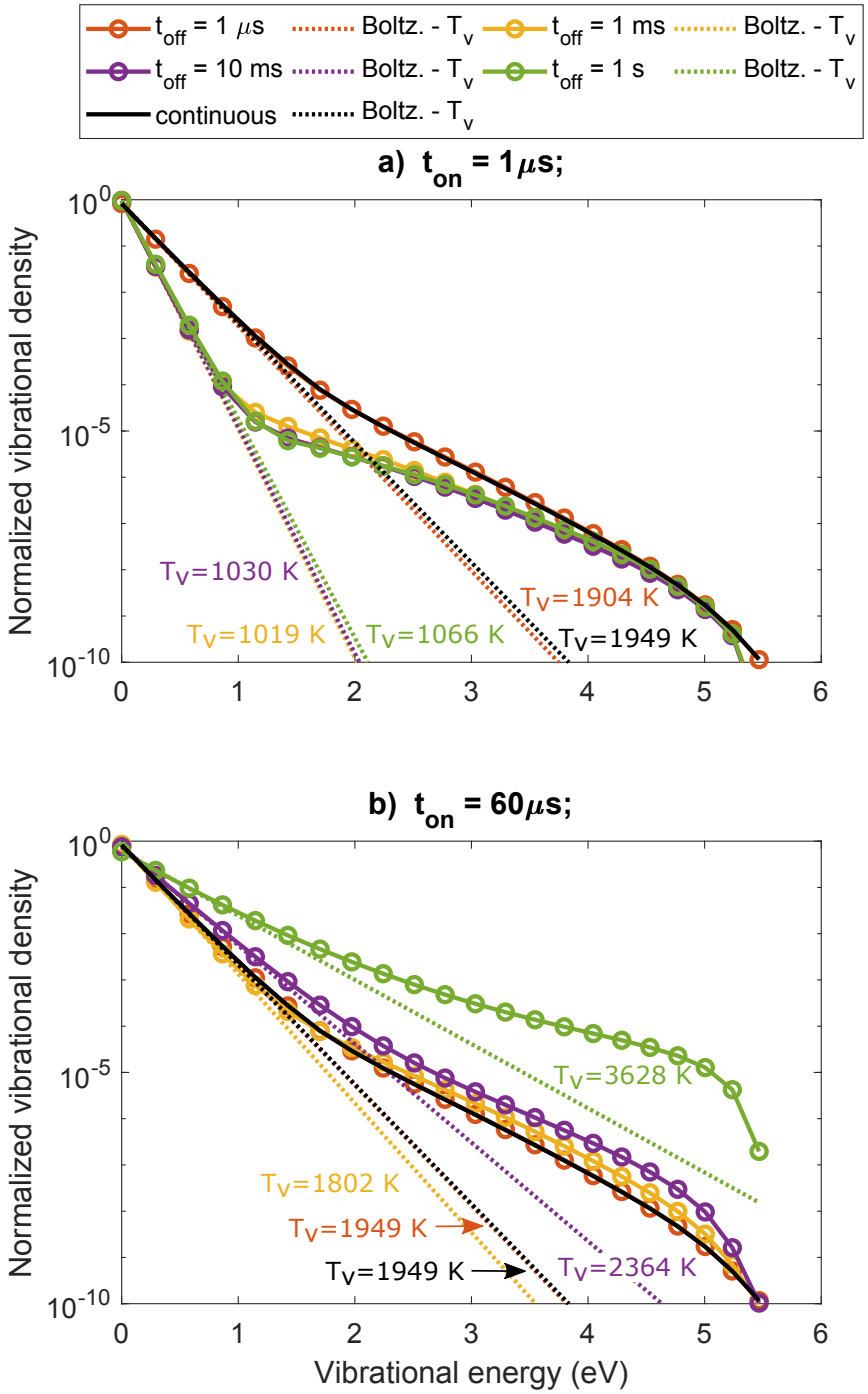

Figure 9: VDFs at the end of the plasma, for two different plasma pulse times, i.e., t_{on} = 1 µs (a, top panel), and t_{on} = 60 µs (b, bottom panels), and for different interpulse times (see legend), at a fixed SEI of 1 eV/molec. The VDF calculated for a continuous plasma (at the same SEI) is illustrated for comparison (black curves). The corresponding Boltzmann distribution functions at the indicated vibrational temperature (reached in each case at the end of the plasma) are also plotted in the same color, to illustrate the degree of over-population of the higher vibrational levels with respect to this equilibrium distribution.

For both plasma pulse times, the VDFs at an interpulse time of 1 µs are virtually the same as the VDF in case of a continuous plasma, with a similar vibrational temperature. Indeed, the interpulse time is insufficient to cause significant relaxation of the VDF (see figure 8). With increasing interpulse time, the evolution of the VDF is different for the two plasma pulse times.

For a plasma pulse time of 1 µs and an interpulse time of 1 ms and above, the VDFs become underpopulated with respect to the continuous plasma. Indeed, the interpulse time is sufficiently long to cause relaxation of the VDF (see figure 8). However, the plasma pulse time is too short to get significant population of the higher vibrational levels (see figure 7). In figure 9, the difference is not large, given that the VDF of the continuous plasma is mostly thermalized as a result of the high gas temperature (1862 K). The underpopulation of the VDF is much more clear in figure S5 of the SI, where the VDFs at half of the plasma are shown.

For a plasma pulse time of 60 µs, the VDF starts getting more populated at higher interpulse times. At an interpulse time of 1 ms, a slight overpopulation of the higher vibrational levels is observed, compared to the VDF of the continuous plasma, despite the slightly lower vibrational temperature (1802 K). This can be correlated with the lower gas temperature (1407 K), allowing for a faster VV relaxation and a slower VT relaxation (see figure 1). For an interpulse time of 10 ms, the gas temperature is even lower (1034 K). However, it can be seen that while the vibrational temperature is higher than the continuous case (2364 K), the population of the higher vibrational levels did not significantly increase. Indeed, while the first vibrational level gets excited, the gas temperature is still too high to allow for a fast overpopulation of the higher vibrational levels (cfr. lower characteristic time scale for VT at higher gas temperature, see figure 1), that were depleted during the interpulse (see figures 4 and 8). This results in a lower overpopulation of the VDF with respect to the equilibrium Boltzmann distribution at T_v (see figure 9 b). Note that a lower population of the higher vibrational levels, despite a higher vibrational

temperature, was also noticed in figure 7 for t = 10 and 80 µs. In the latter case, the gas temperature reached 1005 K, which is similar to the gas temperature mentioned above (1034 K). The slightly higher overpopulation of the VDF for t_{on} = 60 µs and t_{off} = 10 ms, compared to the continuous plasma, is not enough to compensate for the vibrational energy loss between the pulses (see section 2 in the SI) and does not lead to higher energy efficiency, despite a higher average vibrational temperature (see figure 5).

When the interpulse time increases to t_{off} = 1 s, the gas temperature reduce back to 300 K (see figure 4). This results in a larger characteristic time scale, and thus lower rate, for VT relaxation, and a faster VV relaxation. For a plasma pulse time of 60 µs, this results in a large overpopulation, with respect to the continuous plasma, that is again similar to the one in the first plasma pulse (see figure 7). Because at these conditions, higher energy efficiencies are found, it seems that the higher vibrational overpopulation is enough to compensate for the vibrational energy losses between the pulses (see section 2 in the SI).

In figure S5 of the SI, we show the VDFs at the end of the plasma, for plasma pulse time of 10 µs and 100 µs, for different interpulse times. As these plasma pulse times are long enough to reach significant overpopulation (see figure 7), the evolution of the VDFs with increasing interpulse time is similar to the evolution at a plasma pulse time of 60 µs. While the VDFs show a large overpopulation of the higher vibrational levels compared to the VDF of the continuous plasma, for both t_{on} = 10 µs, and t_{on} = 60 µs, at an interpulse time of 1 s, this only leads to a higher energy efficiency for the plasma pulse time of 60 µs (see figure 2). Indeed, due to the shorter plasma pulse time at t_{on} = 10 µs, the number of pulses is higher to reach the same SEI of 1 eV/molec, which will increase the total amount of vibrational energy that is lost (see figure S1 in the SI). Because more vibrational energy is lost, there is less vibrational energy available for vibrationally induced dissociation. In the next section, we will discuss in more detail the dissociation mechanisms.

3.6 Effect of Pulsing on the Dissociation and Recombination Mechanisms

Now that we understand the effect of pulsing on the vibrational and gas temperature and on the shape of the VDF, we can investigate the effect of the different plasma pulse and interpulse times on the CO_2 dissociation and recombination mechanisms. In figure 10, we plot the percentage of CO_2 that is converted by electron impact dissociation (red), dissociation upon collision with a molecule M (blue), and upon collision with an O atom (yellow), as a function of interpulse time, for four different plasma pulse times. The most important recombination mechanism, i.e. recombination of CO and O (purple), is plotted as negative CO_2 conversion. The horizontal lines correspond to the conversion by these four mechanisms in a continuous plasma at the same SEI.

For t_{on}= 1 µs (figure 10 a), all three dissociation mechanisms have the highest CO_2 conversion at t_{off} = 1 µs. At this short interpulse time, the VDF does not relax significantly between two pulses (see figure 8), so there is still enough vibrational build-up through the plasma (see figure 9 a and figure S3 in the SI). This results in the largest contribution to dissociation from collisions of CO_2 with either a molecule M, or an atom O. Given the high activation energy barriers of these reactions,[27] and the relatively low gas temperatures calculated in this work, the energy to overcome this barrier comes from the higher vibrational levels. This is also shown in figure S7 of the SI, where the contribution of the vibrational levels to the overall dissociation is shown.

When the interpulse time increases, the overpopulation of the higher vibrational levels is considerably lower (see figure 9 a and figure S3 in the SI), so vibrationally induced dissociation, upon collision with a molecule M or an atom O, becomes insignificant (see also figure S7 in the SI). Therefore, electron impact dissociation becomes the most important dissociation process, although its absolute value is also quite low and drops upon increasing interpulse time. This is because at the conditions under study (i.e. E/N= 50 Td), most of the electron energy goes into vibrational excitation of CO_2,[27,45] and only a smaller por-

tion goes into direct electron impact dissociation. For longer interpulse times, the VDF relaxes between two pulses (see figure 8), so more of the electron energy is needed at the start of the next pulse to repopulate the VDF, resulting in a lower contribution of electron impact dissociation to the conversion.

Because the dissociation mechanisms have a lower contribution than those of the continuous case for all interpulse times at t_{on}= 1 µs, the recombination is also lower than in the continuous case for all interpulse times. The highest contribution from this reaction happens at short interpulse times, where the overall dissociation is highest.

For t_{on} =10 µs (figure 10 b), vibrationally induced dissociation (upon collision with either another molecule M or an O atom) is dominant for all interpulse times. Just like for t_{on} = 1 µs, the conversion reaches its maximum for short interpulse times (i.e. t_{off} = 1 µs), because the VDF is not drastically depleted between the pulses at these short interpulse times. The conversion is higher than for t_{on} = 1 µs, since there are less pulses in total (for the same fixed SEI), and thus less overall vibrational energy loss (see figure S1 of the SI). When the interpulse time increases, all three dissociation mechanisms first yield less conversion, but above t_{off} = 10 ms, they again become more important. This is consistent with the increase in energy efficiency, observed in figure 2, and can be explained by the lower gas temperature, which allows for a higher population of the VDF near the end of the plasma, compared to a continuous plasma (see figure S5 in the SI). The contribution of electron impact dissociation is again quite small and drops upon longer interpulse times, like with t_{on} = 1 µs, for the same reason.

The recombination is high at short interpulse times, similarly to figure 10 (a). The recombination is slightly lower than in the continuous case, which can be correlated to the lower conversion. However, at long interpulse times, the recombination becomes higher than in the continuous case, while the conversion is lower. It was seen in ref.[29] that recombination is very prominent in the afterglow, because the O atoms formed in the plasma are less used in vibrational-induced dissociation due to the lower vibrational

temperature. The higher contribution of this process at t_{on} = 10 µs and t_{off} = 1 s can be explained by the multiple interpulses. The increase was not observed at short interpulse times, since these were too short to increase the effect of the recombination.

It is clear from figure 10 (a,b) that these very short plasma pulse times yield a significantly lower conversion by all three processes than the continuous plasma, for all interpulse times, except for the shortest interpulse times, where the role of electron impact dissociation is comparable to that for a continuous plasma. This picture corresponds to figure 2, where the overall conversion and energy efficiency were lower than for the continuous plasma.

For t_{on} = 60 µs and t_{on} = 100 µs, the conversion by all three processes is comparable to the continuous plasma for $t_{off} \leq 10$ ms. When $t_{off} \geq 100$ ms, the conversion by vibrationally induced dissociation, upon collision with a molecule M or an atom O, becomes higher than that for the continuous plasma. This is correlated with the lower number of pulses, and hence lower total vibrational temperature loss (see figure S1 in the SI), at these plasma pulse times, combined with a significant overpopulation of the higher vibrational levels, with respect to the continuous plasma, close to the end of the plasma (see figure 9). Similarly to the conversion, the contribution of the recombination process follows that of the continuous plasma for short interpulse times. For longer interpulse times, the recombination becomes higher than that of the continuous case, which can be explained by the multiple pulses, and the higher contribution of the dissociation mechanisms. However, the higher recombination is not enough to compensate for the increase in dissociation, thus explaining the higher conversion and energy efficiencies in figure 2.

3.7 Influence of Cooling on the Pulsing Effect

From sections 3.3, 3.4, and 3.5, we concluded that the reduction of the gas temperature resulted in a higher average vibrational temperature, and a higher overpopulation of the higher vibrational levels, which is beneficial for vibrationally induced dissociation (see

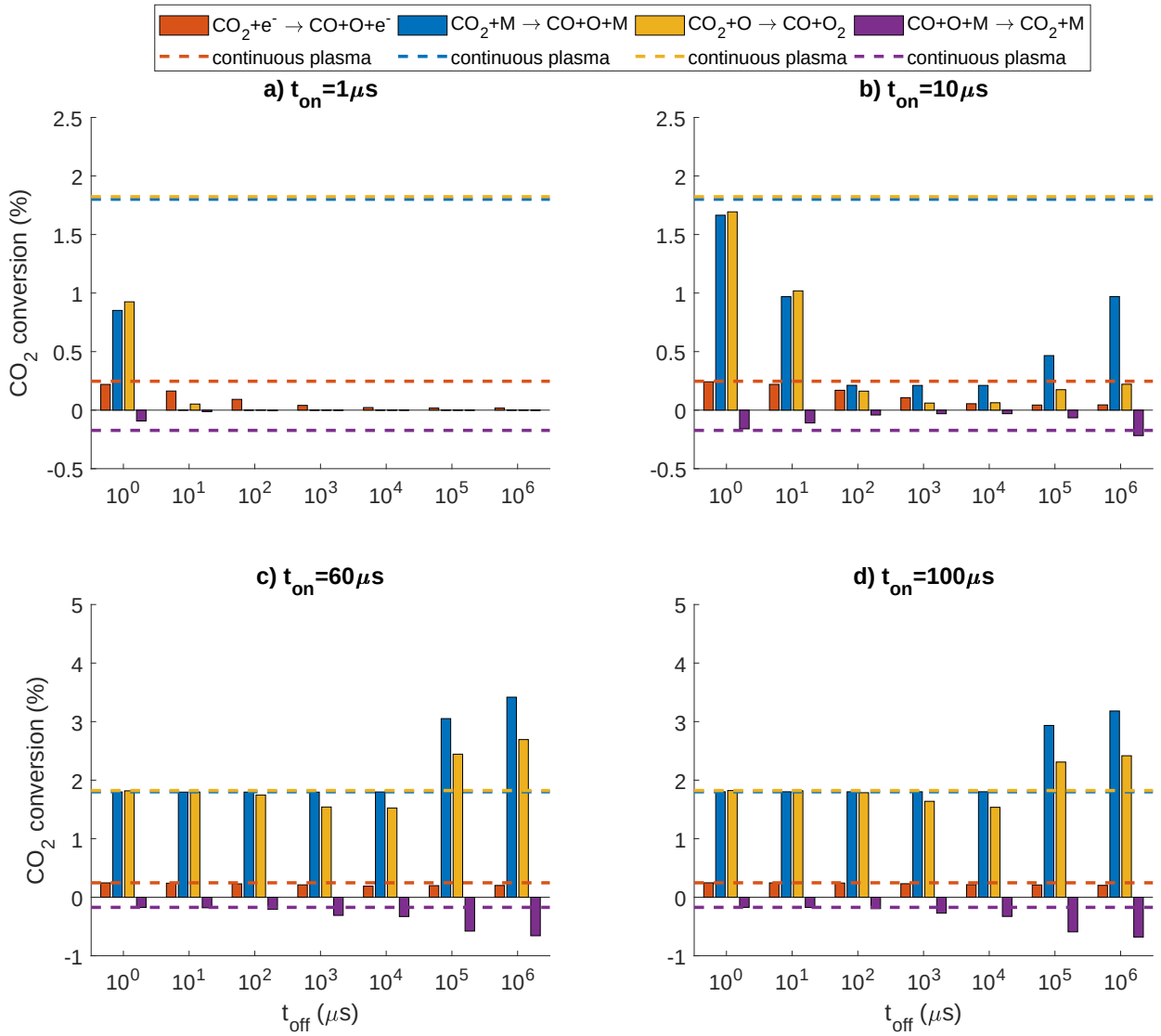

Figure 10: Percentage of converted CO_2 by the three main dissociation reactions: electron impact dissociation (red), dissociation upon collision with a molecule M (blue) and dissociation upon collision with an O atom (yellow). The major recombination reaction, forming CO_2 is also plotted (purple, negative value). The dashed lines represent the respective conversions and recombination for a continuous plasma at the same SEI of 1 eV/molec.

section 3.6). Thus, we may conclude that a lower gas temperature has a beneficial effect on the dissociation, and therefore we investigate here the effect of additional wall cooling on the energy efficiency, for a plasma pulse time of t_{on} = 60 µs, and different interpulse times. This is illustrated in figure 11, for the standard case (no additional cooling: λ_{add} = 0), and three different cooling rates, defined by additional thermal conductivities, λ_{add} = 0.01, 0.1, and 1 $Wm^{-1}K^{-1}$ (see eq. 7 above). For higher cooling rates, the improvement in energy efficiency with respect to a continuous plasma happens at shorter interpulse times. Indeed, for λ_{add} =0.1 $Wm^{-1}K^{-1}$, the energy efficiency already shows an improvement at t_{off} = 10 ms, while for λ_{add} =1 $Wm^{-1}K^{-1}$, this occurs at t_{off} = 1 ms already. This means that additional cooling can be used to tune the interpulse time at which the full potential of plasma pulsing can be exploited.

3.8 Influence of the Ionization Degree and Reduced Electric Field on the Pulsing Effect

Up till now, we have only discussed the effect of pulsing at an ionization degree of 10^{-6} and a reduced electric field of 50 Td, which are characteristic for so-called warm plasmas, like MW and GA discharges.[3,8,37] In this section, we will evaluate the effect of the ionization degree and the reduced electric field on the potential of plasma pulsing. In figure 12, we vary the ionization degree between 2×10^{-7} and 10^{-5} at a reduced electric field of 50 Td. The blue bars are the energy efficiencies for a continuous plasma, while the red bars represent the maximum energy efficiency (evaluated for different plasma pulse and interpulse times) that can be added by pulsing. For ionization degrees of 5×10^{-7} and 10^{-6}, pulsing can indeed increase the energy efficiency of CO_2 dissociation, upon selecting the right values of plasma pulse and interpulse times (cf. figure 2). However, at both lower and higher ionization degrees, pulsing seems not to increase the energy efficiency, which can be explained as follows.

The reason why the energy efficiency does not increase at the high ionization degree of

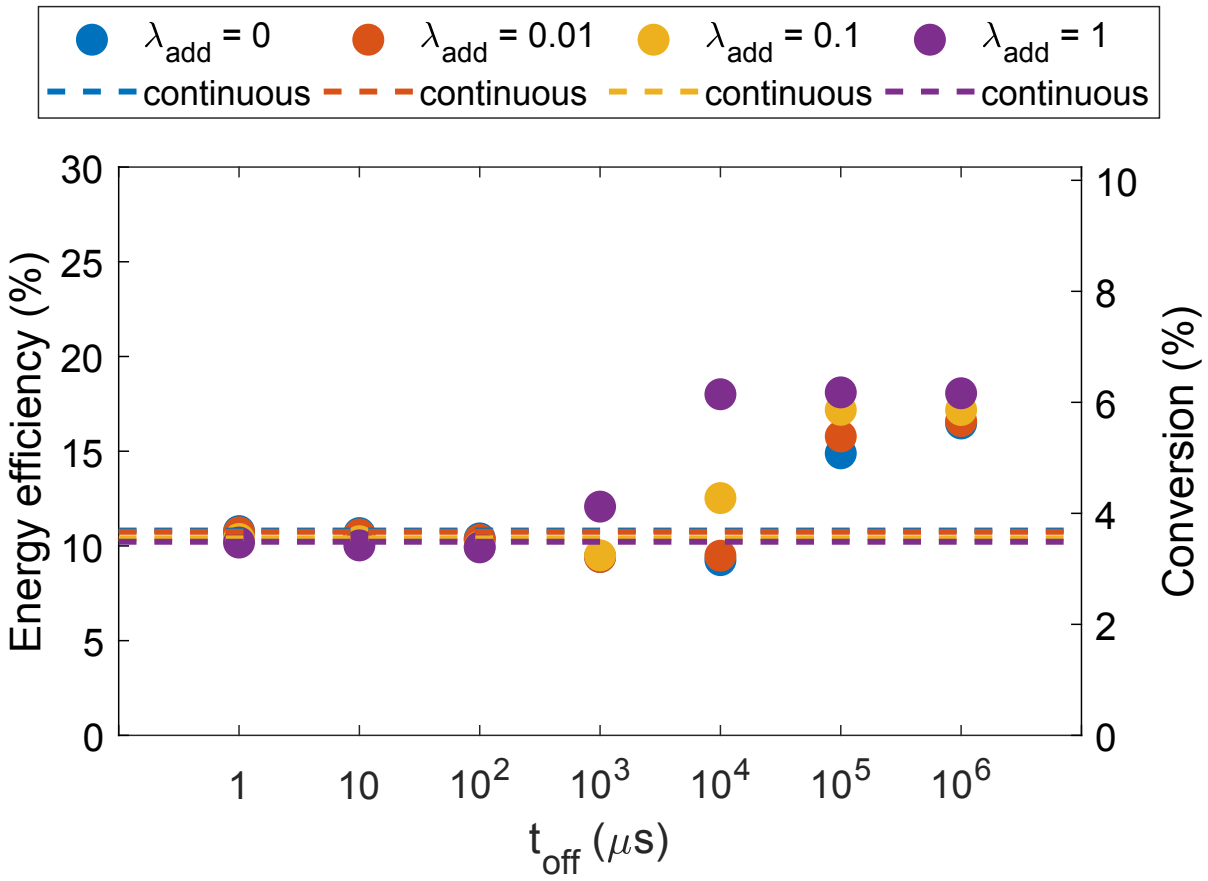

Figure 11: Energy efficiency and conversion as a function of interpulse time (t_{off}), for a plasma pulse time t_{on} = 60 µs, and for different cooling rates, as defined by the additional thermal conductivity, λ_{add} (in $Wm^{-1}K^{-1}$), besides the basic case (no additional cooling). The dashed horizontal lines correspond to the continuous plasma cases.

1×10^{-5} lies in the much faster rise of the vibrational temperature, with respect to the gas temperature, due to the shorter time scales of electron impact vibrational excitation (see figure 1). This is shown in figure S6 of the SI where the time-evolutions of the vibrational and gas temperature are plotted at different ionization degrees. Since the vibrational temperature rises much faster than the gas temperature, the latter does not reach high enough values to thermalize the vibrational temperature, which therefore increases until the end of the plasma. Since no thermalization of the vibrational temperature occurs during the continuous plasma, pulsing will not be able to increase the vibrational temperature, and will therefore not be able to improve the energy efficiency. For $d_i = 5 \times 10^{-6}$, thermalization does start to occur. However, the energy efficiency does not improve, as this thermalization happens closer to the end of the plasma, which prevents pulsing from improving the energy efficiency. In figure 12, ionization degrees higher than the dashed vertical line have a vibrational temperature increase until the end of the plasma.

At a low ionization degree of $d_i = 2 \times 10^{-7}$, the vibrational temperature does reach a maximum value, after which it thermalizes (see figure S6 in the SI). However, pulsing cannot increase the energy efficiency (see figure 12). This can be explained by the contribution of the different dissociation mechanisms, shown in figure 13 for different plasma pulse times, and an interpulse time of 1 s. At low ionization degrees, the characteristic time scale of electron impact vibrational excitation is much longer (see for $d_i = 10^{-7}$ in figure 1), resulting in a smaller contribution from vibrationally induced dissociation upon collision with a molecule M or an atom O. As can be seen in figure 13, electron impact dissociation becomes the most important dissociation mechanism. While pulsing increases the dissociation upon collision with a molecule M (see t_{on} = 100 - 1000 µs in figure 13), this rise is compensated by the negative effect of pulsing on electron impact dissociation (as was also seen in figure 10). The lower total contribution from these two reactions also lowers the dissociation upon collision with an atom O, as they provide the O atoms for this reaction. The reduced contribution of electron impact dissociation and dissociation

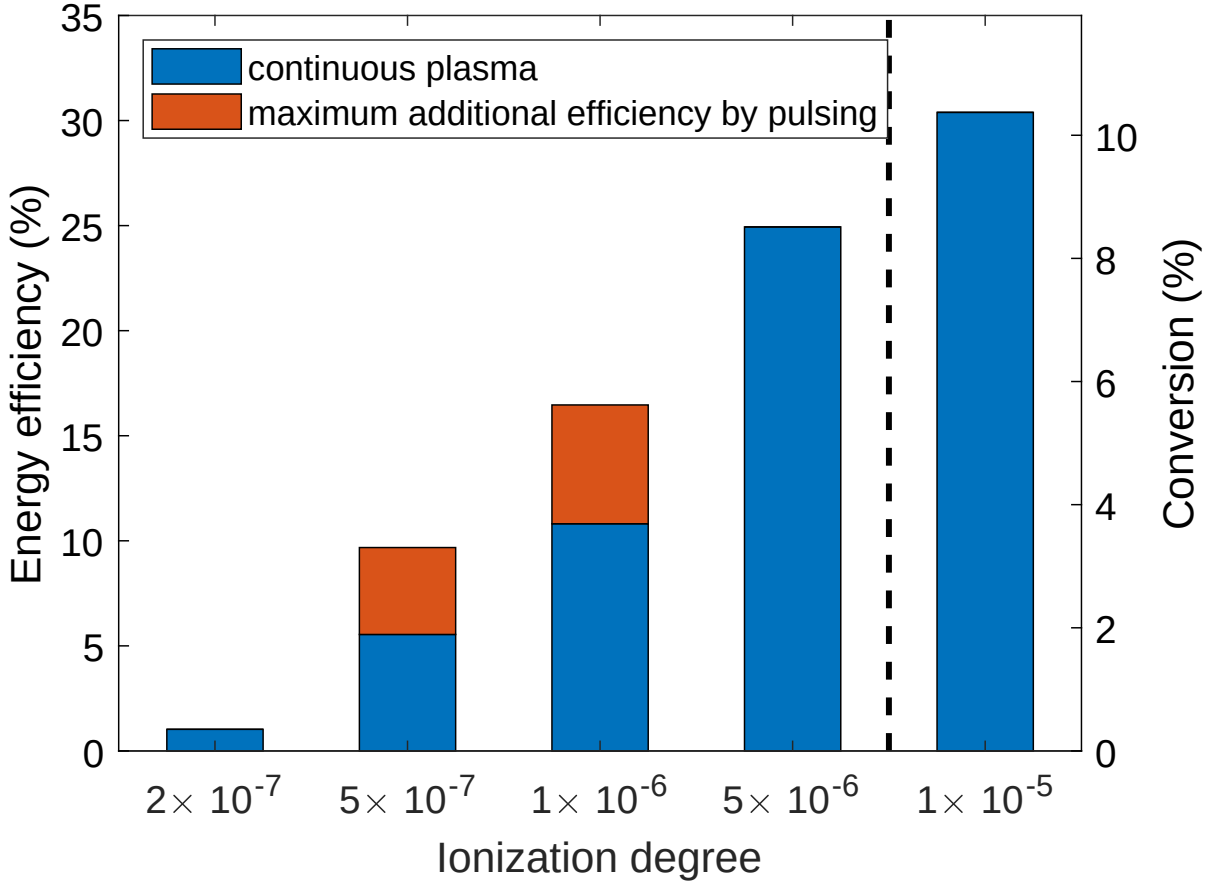

Figure 12: Energy efficiency and conversion of a continuous plasma (blue bars), and maximum additional energy efficiency caused by pulsing, for different ionization degrees, at an interpulse time of 1 s, and a reduced electric field of 50 Td. At ionization degrees higher than the dashed line, no thermalization of the vibrational temperature occurs for this total SEI.

by collision with an atom O will therefore not lead to higher energy efficiencies, with respect to the continuous plasma.

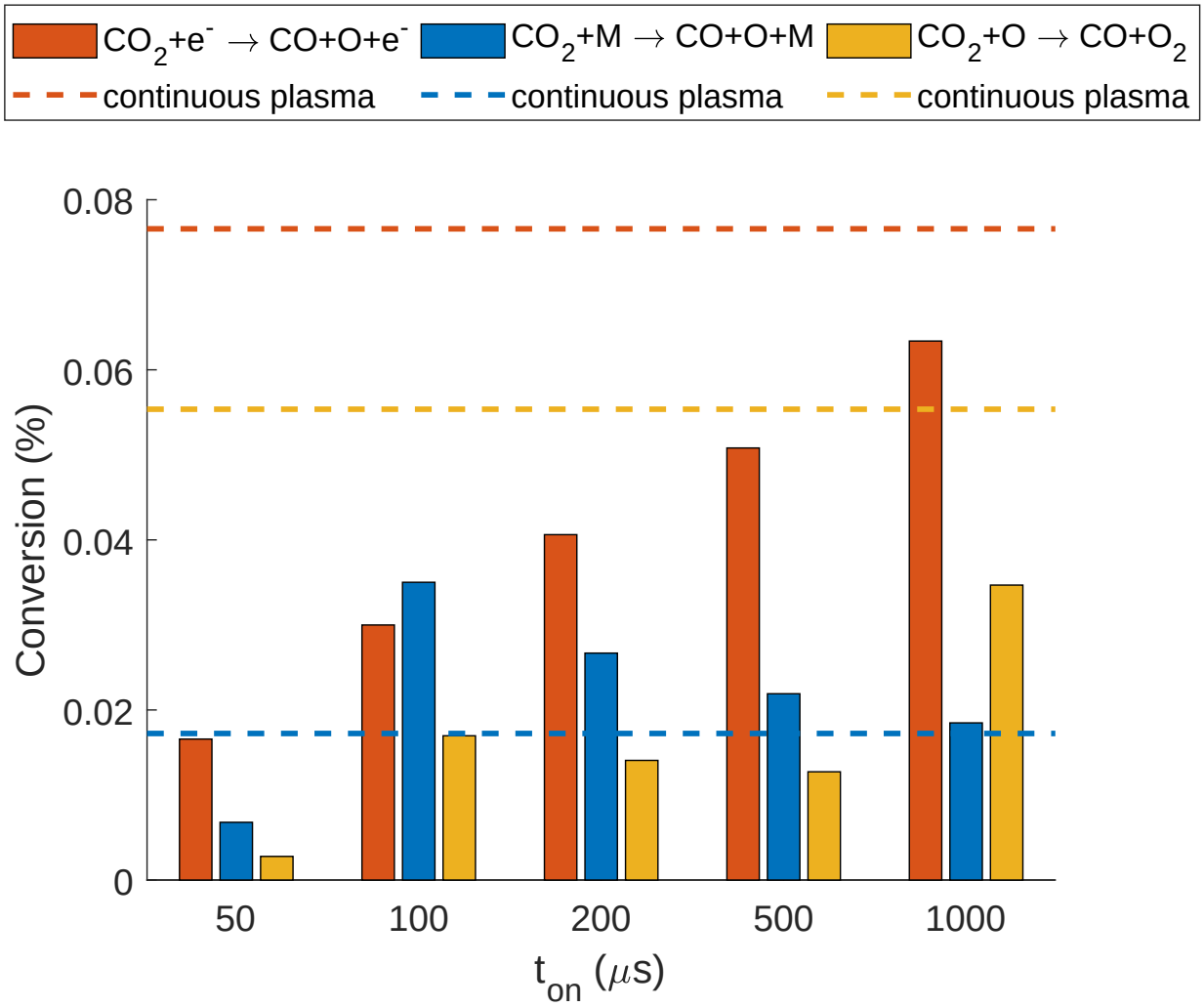

Figure 13: CO_2 conversion by the three main dissociation reactions: electron impact dissociation (red), dissociation upon collision with a molecule M (blue) and upon collision with an O atom (yellow), for different plasma pulse times and an interpulse time of 1 s, a reduced electric field of 50 Td and an ionization degree of 2×10^{-7}. The dashed horizontal lines represent the respective conversions of a continuous plasma at the same SEI.

When the reduced electric field increases, vibrationally induced dissociation becomes less important due to the lower amount of electron energy that goes to the vibrational modes.[27] Figure 14 illustrates the effect of the latter on the additional energy efficiency created by pulsing the plasma, for 100 Td and 150 Td. At a reduced electric field of 100

Td (corresponding to an electron temperature of about 2 eV), pulsing increases the energy efficiency at an ionization degree of 5×10^{-7} and 10^{-6} (see figure 14 a). The increase at $d_i = 10^{-6}$ is small, because thermalization occurs closer to the end of the plasma. At a reduced electric field of 150 Td (and corresponding electron temperature of 2.8 eV), the energy efficiency is only enhanced at an ionization degree of 10^{-7}. However, it can be seen in figure S8 that the vibrational temperature thermalizes in the first half of the plasma. Hence, the small increase in energy efficiency is a result of the smaller influence of vibrationally induced dissociation at higher reduced electric fields.[27]

For high and low ionization degrees, pulsing the plasma also does not lead to higher energy efficiency at higher reduced electric fields of 100 Td and 150 Td. Similar explanations as the ones that were given for a reduced electric field of 50 Td also apply. Indeed, at high ionization degrees, the vibrational temperature also increases until the end of the plasma (see figures S7 and S8 of the SI), while at low ionization degrees, the negative effect of pulsing on the most prominent dissociation mechanism, i.e. electron impact dissociation, can not be compensated by the positive effect on the vibrationally induced dissociation by collision with a molecule M. This is shown in figures S10 and S11 of the SI for $d_i = 10^{-7}$ at 100 Td and $d_i = 5 \times 10^{-8}$ at 150 Td, respectively.

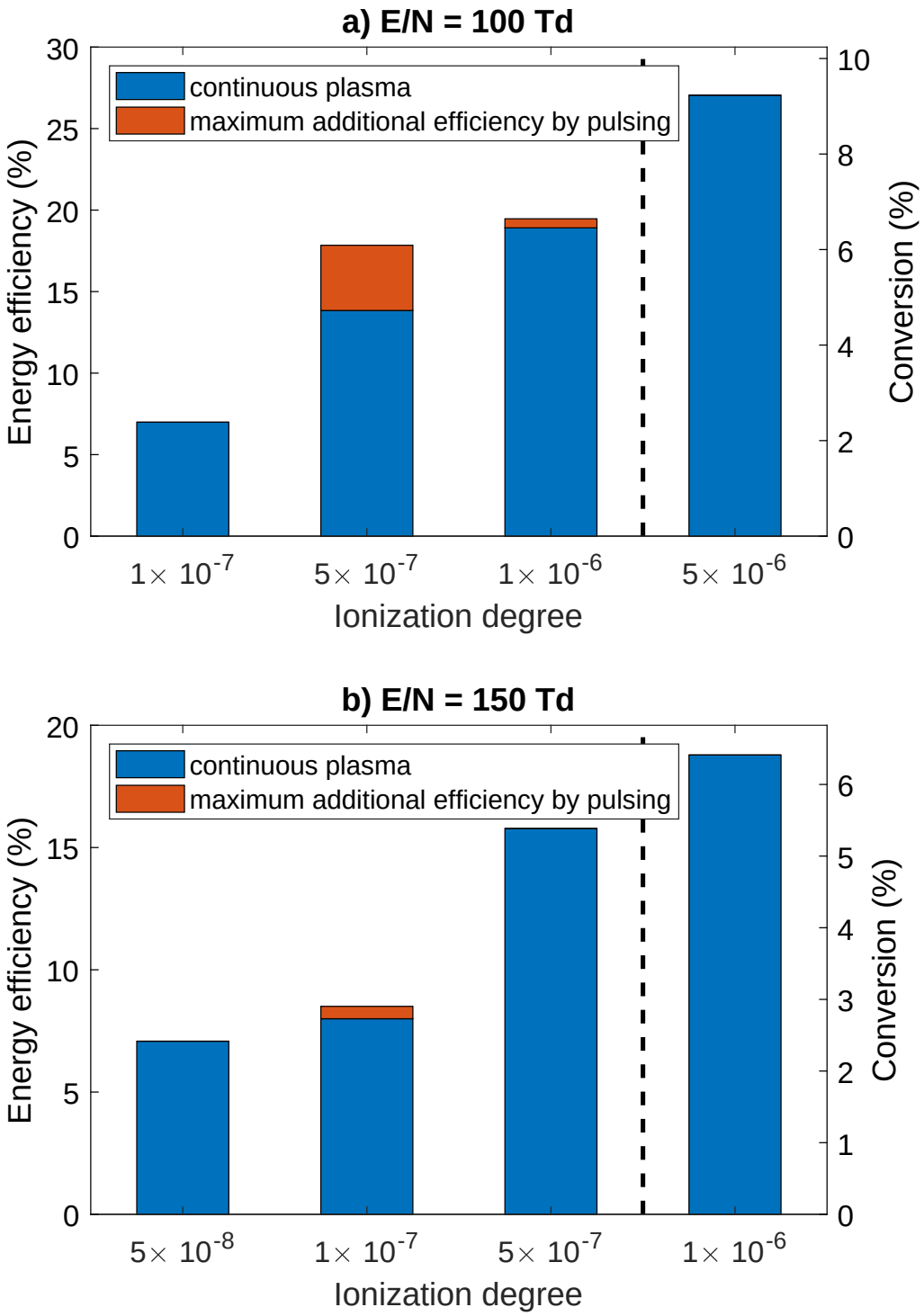

Figure 14: Energy efficiency and conversion of a continuous plasma (blue bars), and maximum additional energy efficiency, caused by pulsing, for different ionization degrees, at an interpulse time of 1 s, and for a reduced electric field of a) 100 Td, and b) 150 Td. At ionization degrees higher than the dashed line, no thermalization of the vibrational temperature occurs for this total SEI.

4 Conclusions

We have demonstrated the potential of plasma pulsing for improving the energy efficiency of CO_2 dissociation in a non-equilibrium plasma, by means of a 0D chemical kinetics model with self-consistent gas temperature calculation. At a reduced electric field of 50 Td, an ionization degree of 10^{-6}, and a total SEI of 1eV/molec, our model predicts a drop in energy efficiency for short plasma pulse and interpulse times (i.e. $t_{on} \leq 10$ µs, and $t_{off} \leq 10$ ms), while an improvement in energy efficiency was calculated at longer plasma pulse and interpulse times.

To explain these results, we studied the vibrational and gas temperature evolution as a function of time during and after the pulse. The vibrational temperature quickly rises, but drops again after a maximum is reached, while the gas temperature rises more slowly, but shows a continuous increase during and even after the pulse, and only drops for long enough interpulse times. The plasma pulse time for which the highest energy efficiency was found (60 µs) corresponds to the time at which the vibrational temperature reaches its maximum. For shorter plasma pulse times, this maximum could not be reached, while at longer plasma pulse times, thermalization due to the high gas temperature results in a strong drop in vibrational temperature. This effect is correlated with the shorter characteristic time of VT relaxation at higher gas temperatures. At interpulse times above t_{off} = 1 ms, the vibrational and gas temperature reach an equilibrium, and both reach room temperature at t_{off} = 1 s. A maximum energy efficiency of 16.5% (compared to 10.8% for a continuous plasma at the same conditions) was obtained for a plasma pulse time t_{on} = 60 µs, and an interpulse time t_{off} = 1 s. We want to note that the absolute values in this work are subject to some uncertainties, as a result of the uncertainties that exist on the rate coefficients. It is thus more important to focus on the trends they reveal, as they are typically not affected by these uncertainties.[42]

The effect of pulsing was also reflected in the evolution of the VDF. During the pulse, the higher vibrational levels start to get populated, but when the gas temperature be-

comes about 1000 K, the higher vibrational levels, which are needed for efficient vibrationally induced dissociation, start to get depleted. Hence, for plasma pulse times of 60 µs, the VDF is still overpopulated by the end of the pulse, but it quickly thermalizes after the pulse, and for interpulse times t_{off} = 1 ms, the VDF returns to a Boltzmann distribution, in equilibrium with the translational (gas) temperature.

We also compared the VDF at the end of the plasma (when the total SEI of 1 eV/molec was reached) for different plasma pulse and interpulse times. For short interpulse times, the VDF closely resembles that of a continuous plasma, which is nearly thermalized because of the higher gas temperature. However, for longer interpulse times, the reduction in gas temperature was enough to allow a considerable overpopulation of the vibrational levels with respect to the continuous plasma. This overpopulation was the highest for t_{off} = 1 s, at which the highest energy efficiencies were found. However, the plasma pulse time needs to be long enough (ca. 60 µs), to fully exploit the beneficial effect of plasma pulsing, since the VDF needs this time to fully build up during the pulses, and a lower number of pulses reduces the losses of vibrational energy in between the pulses.

By evaluating the role of the various CO_2 dissociation processes, our model reveals that the higher energy efficiency upon pulsing (at long enough plasma pulse and interpulse times) is due to an increased contribution from vibrationally induced dissociation (mainly CO_2+M $\rightarrow$ CO+O+M, but also CO_2 + O $\rightarrow$ CO+O_2).

We also studied the effect of additional plasma cooling on the pulsing effect. Our model shows that for higher plasma cooling, the beneficial effects of pulsing already occur at shorter interpulse times, which is logical, as the gas temperature drops more quickly.

Finally, we evaluated the pulsing effect for different ionization degrees and reduced electric fields. At high ionization degrees, the vibrational temperature rises much faster than the gas temperature, resulting in higher energy efficiencies in a continuous plasma. Hence, as no thermalization of the vibrational levels occurs (due to the lower gas temperature), plasma pulsing cannot further improve the energy efficiency. At low ionization

degrees and higher reduced electric fields, vibrationally induced dissociation is of lower importance, so pulsing has again no (or only a minor) effect on the energy efficiency. Therefore, our model reveals that pulsing can significantly enhance the energy efficiency for ionization degrees around 5×10^{-7} - 10^{-6}, and low reduced electric fields of about 50 Td and 100 Td.

In summary, our model provides interesting insights in how plasma pulsing can compensate for the negative effect of thermalization of the VDF, and how it can be used to increase the vibrational-translational non-equilibrium in CO_2 plasmas, and thus to optimize the role of vibrationally induced dissociation as the most energy efficient CO_2 dissociation pathway.

Acknowledgement

This research was supported by the FWO project (grant G.0383.16N). The calculations were performed using the Turing HPC infrastructure at the CalcUA core facility of the Universiteit Antwerpen (UAntwerpen), a division of the Flemish Supercomputer Center VSC, funded by the Hercules Foundation, the Flemish Government (department EWI) and the UAntwerpen. We also like to thank N. Britun (ChIPS) for the interesting discussions.

Supporting Information Available

The supporting information is available free of charge and contains:

- Reactions included in the models as well as their rate coefficients or cross sections.
- Total Temperature Gains and Losses by Plasma Pulsing.
- Temporal Evolution of the Gas Temperature.

- VDF Halfway the Plasma for t_{on} = 1 and 10 µs.
- VDF at the End of the Plasma for t_{on} = 10 and 100 µs.
- Relative Contribution of the Individual Vibrational Levels to Dissociation
- Time-evolution of the Vibrational and Gas Temperature in a Continuous Plasma for Different Ionization Degrees and Reduced Electric Fields.
- Dissociation Mechanisms for Different Reduced Electric Fields at a Low Ionization Degree.

References

(1) REN21, Renewables 2018: Global Status Report. 2018; `http://www.ren21.net/wp-content/uploads/2018/06/17-8652\_GSR2018\_FullReport\_web\_final\_.pdf`.

(2) Fridman, A. *Plasma Chemistry*; Cambridge University Press: New York, USA, 2008.

(3) Snoeckx, R.; Bogaerts, A. Plasma Technology - a Novel Solution for CO_2 Conversion? *Chem. Soc. Rev.* **2017**, *46*, 5805–5863.

(4) Silva, T.; Britun, N.; Godfroid, T.; Snyders, R. Optical Characterization of a Microwave Pulsed Discharge used for Dissociation of CO_2. *Plasma Sources Sci. Technol.* **2014**, *23*, 025009.

(5) Spencer, L. F.; Gallimore, A. D. Efficiency of CO_2 Dissociation in a Radio-Frequency Discharge. *Plasma Chem. Plasma Process.* **2011**, *31*, 79–89.

(6) Bongers, W.; Bouwmeester, H.; Wolf, B.; Peeters, F.; Welzel, S.; van den Bekerom, D.; den Harder, N.; Goede, A.; Graswinckel, M.; Groen, P. W. et al. Plasma-Driven Dissociation of CO_2 for Fuel Synthesis. *Plasma Processes Polym.* **2016**, 1–8.

(7) Belov, I.; Vermeiren, V.; Paulussen, S.; Bogaerts, A. Carbon Dioxide Dissociation in a Microwave Plasma Reactor Operating in a Wide Pressure Range and Different Gas Inlet Configurations. *J. CO_2 Util.* **2018**, *24*, 386–397.

(8) den Harder, N.; van den Bekerom, D. C. M.; Al, R. S.; Graswinckel, M. F.; Palomares, J. M.; Peeters, F. J. J.; Ponduri, S.; Minea, T.; Bongers, W. A.; van de Sanden, M. C. M. et al. Homogeneous CO_2 Conversion by Microwave Plasma: Wave Propagation and Diagnostics. *Plasma Processes Polym.* **2017**, *14*, 1600120.

(9) Britun, N.; Silva, T.; Chen, G.; Godfroid, T.; van der Mullen, J.; Snyders, R. Plasma-assisted CO_2 Conversion: Optimizing Performance via Microwave Power Modulation. *J. Phys. D: Appl. Phys.* **2018**, *51*, 144002.

(10) Nunnally, T.; Gutsol, K.; Rabinovich, A.; Fridman, A.; Gutsol, A.; Kemoun, A. Dissociation of CO_2 in a Low Current Gliding Arc Plasmatron. *J. Phys. D: Appl. Phys.* **2011**, *44*, 274009.

(11) Ramakers, M.; Trenchev, G.; Heijkers, S.; Wang, W.; Bogaerts, A. Gliding Arc Plasmatron: Providing an Alternative Method for Carbon Dioxide Conversion. *ChemSusChem* **2017**, *10*, 2642–2652.

(12) Indarto, A.; Yang, D. R.; Choi, J. W.; Lee, H.; Song, H. K. Gliding Arc Plasma Processing of CO_2 Conversion. *J. Hazard. Mater.* **2007**, *146*, 309–315.

(13) Belov, I.; Paulussen, S.; Bogaerts, A. Appearance of a Conductive Carbonaceous Coating in a CO_2 Dielectric Barrier Discharge and its Influence on the Electrical Properties and the Conversion Efficiency. *Plasma Sources Sci. Technol.* **2016**, *25*, 015023.

(14) Michielsen, I.; Uytdenhouwen, Y.; Pype, J.; Michielsen, B.; Mertens, J.; Reniers, F.; Meynen, V.; Bogaerts, A. CO_2 Dissociation in a Packed Bed DBD Reactor: First Steps Towards a Better Understanding of Plasma Catalysis. *Chem. Eng. J.* **2017**, *326*, 477–488.

(15) Paulussen, S.; Verheyde, B.; Tu, X.; De Bie, C.; Martens, T.; Petrovic, D.; Bogaerts, A.; Sels, B. Conversion of Carbon Dioxide to Value-Added Chemicals in Atmospheric Pressure Dielectric Barrier Discharges. *Plasma Sources Sci. Technol.* **2010**, *19*, 034015 1–6.

(16) Aerts, R.; Somers, W.; Bogaerts, A. Carbon Dioxide Splitting in a Dielectric Barrier Discharge Plasma: A Combined Experimental and Computational Study. *ChemSusChem* **2015**, *8*, 702–716.

(17) Uytdenhouwen, Y.; Van Alphen, S.; Michielsen, I.; Meynen, V.; Cool, P.; Bogaerts, A. A Packed-bed DBD Micro Plasma Reactor for CO_2 Dissociation: Does Size Matter? *Chem. Eng. J.* **2018**, *348*, 557–568.

(18) Wang, J.-Y.; Xia, G.-G.; Huang, A.; Suib, S. L.; Hayashi, Y.; Matsumoto, H. CO_2 Decomposition Using Glow Discharge Plasmas. *J. Catal.* **1999**, *185*, 152–159.

(19) Trenchev, G.; Nikiforov, A.; Wang, W.; Kolev, S.; Bogaerts, A. Atmospheric Pressure Glow Discharge for CO_2 Conversion: Model-based Exploration of the Optimum Reactor Configuration. *Chem. Eng. J.* **2019**, *362*, 830–841.

(20) Horváth, G.; Skalný, J. D.; Mason, N. J. FTIR Study of Decomposition of Carbon Dioxide in DC Corona Discharges. *J. Phys. D: Appl. Phys.* **2008**, *41*, 225207.

(21) Wen, Y.; Jiang, X. Decomposition of CO_2 Using Pulsed Corona Discharges Combined with Catalyst. *Plasma Chem. Plasma Process.* **2001**, *21*, 665–678.

(22) Moss, M. S.; Yanallah, K.; Allen, R. W. K.; Pontiga, F. An Investigation of CO_2 Splitting Using Nanosecond Pulsed Corona Discharge: Effect of Argon Addition on CO_2 Conversion and Energy Efficiency. *Plasma Sources Sci. Technol.* **2017**, *26*, 035009.

(23) Martini, L. M.; Gatti, N.; Dilecce, G.; Scotoni, M.; Tosi, P. Laser Induced Fluores-

cence in Nanosecond Repetitively Pulsed Discharges for CO_2 Conversion. *Plasma Phys. Controlled Fusion* **2018**, *60*, 014016.

(24) Martini, L. M.; Lovascio, S.; Dilecce, G.; Tosi, P. Time-Resolved CO_2 Dissociation in a Nanosecond Pulsed Discharge. *Plasma Chem. Plasma Process.* **2018**, *38*, 707–718.

(25) Kozák, T.; Bogaerts, A. Splitting of CO_2 by Vibrational Excitation in Non-Equilibrium Plasmas: a Reaction Kinetics Model. *Plasma Sources Sci. Technol.* **2014**, *23*, 045004.

(26) Pietanza, L. D.; Colonna, G.; D'Ammando, G.; Capitelli, M. Time-Dependent Coupling of Electron Energy Distribution Function, Vibrational Kinetics of the Asymmetric Mode of CO_2 and Dissociation, Ionization and Electronic Excitation Kinetics under Discharge and Post-Discharge Conditions. *Plasma Phys. Controlled Fusion* **2017**, *59*, 014035.

(27) Berthelot, A.; Bogaerts, A. Pinpointing Energy Losses in CO_2 Plasmas - Effect on CO_2 Conversion. *J. CO_2 Util.* **2018**, *24*, 479–499.

(28) Kozák, T.; Bogaerts, A. Evaluation of the Energy Efficiency of CO_2 Conversion in Microwave Discharges using a Reaction Kinetics Model. *Plasma Sources Sci. Technol.* **2015**, *24*, 015024.

(29) Berthelot, A.; Bogaerts, A. Modeling of CO_2 Splitting in a Microwave Plasma: How to Improve the Conversion and Energy Efficiency. *J. Phys. Chem. C* **2017**, *121*, 8236–8251.

(30) Heijkers, S.; Bogaerts, A. CO_2 Conversion in a Gliding Arc Plasmatron: Elucidating the Chemistry through Kinetic Modeling. *J. Phys. Chem. C* **2017**, *121*, 22644–22655.

(31) van den Bekerom, D. C. M.; Linares, J. M. P.; Verreycken, T.; van Veldhuizen, E. M.; Nijdam, S.; Berden, G.; Bongers, W. A.; van de Sanden, M. C. M.; van Rooij, G. J. The Importance of Thermal Dissociation in CO_2 Microwave Discharges Investigated by

Power Pulsing and Rotational Raman Scattering. *Plasma Sources Sci. Technol.* **2019**, *28*, 055015.

(32) Ozkan, A.; Dufour, T.; Silva, T.; Britun, N.; Snyders, R.; Reniers, F.; Bogaerts, A. DBD in Burst Mode: Solution for more Efficient CO_2 Conversion? *Plasma Sources Sci. Technol.* **2016**, *25*, 055005.

(33) Ozkan, A.; Dufour, T.; Silva, T.; Britun, N.; Snyders, R.; Bogaerts, A.; Reniers, F. The Influence of Power and Frequency on the Filamentary Behavior of a Flowing DBD - Application to the splitting of CO_2. *Plasma Sources Sci. Technol.* **2016**, *25*, 025013.

(34) Pancheshnyi, S.; Eismann, B.; Hagelaar, G.; Pitchford, L. ZDPlasKin. 2008; `http://www.zdplaskin.laplace.univ-tlse.fr`.

(35) Hagelaar, G. J. M.; Pitchford, L. C. Solving the Boltzmann Equation to Obtain Electron Transport Coefficients and Rate Coefficients for Fluid Models. *Plasma Sources Sci. Technol.* **2005**, *14*, 722–733.

(36) Asisov, R. I.; Vakar, A. K.; Jivotov, V. K.; Krotov, M. F.; Zinoviev, O. A.; Potapkin, B. V.; Rusanov, A. A.; Rusanov, V. D.; Fridman, A. A. Non-Equilibrium Plasma-Chemical Process of CO_2 Decomposition in a Supersonic Microwave Discharge. *Proc. USSR Acad. Sci.* **1983**, *271*, 94–98.

(37) Wang, W.; Mei, D.; Tu, X.; Bogaerts, A. Gliding Arc Plasma for CO_2 Conversion: Better Insights by a Combined Experimental and Modelling Approach. *Chem. Eng. J.* **2017**, *330*, 11–25.

(38) Bogaerts, A.; Wang, W.; Berthelot, A.; Guerra, V. Modeling Plasma-Based CO_2 Conversion : Crucial Role of the Dissociation Cross Section. *Plasma Sources Sci. Technol.* **2016**, *25*, 1–23.

(39) Bogaerts, A.; Kozák, T.; van Laer, K.; Snoeckx, R. Plasma-based Conversion of CO_2 : Current Status and Future Challenges. *Faraday Discuss.* **2015**, *183*, 217–232.

(40) Wilcox, D. C. *Turbulence Modeling for CFD*, 3rd ed.; DCW industries Inc.: La Canada, USA, 2006.

(41) Trenchev, G.; Kolev, S.; Wang, W.; Ramakers, M.; Bogaerts, A. CO_2 Conversion in a Gliding Arc Plasmatron: Multidimensional Modeling for Improved Efficiency. *J. Phys. Chem. C* **2017**, *121*, 24470–24479.

(42) Berthelot, A.; Bogaerts, A. Modeling of CO_2 Plasma: Effect of Uncertainties in the Plasma Chemistry. *Plasma Sources Sci. Technol.* **2017**, *26*, 115002.

(43) Berthelot, A.; Bogaerts, A. Modeling of Plasma-Based CO_2 Conversion: Lumping of the Vibrational Levels. *Plasma Sources Sci. Technol.* **2016**, *25*, 045022.

(44) Koelman, P.; Heijkers, S.; Tadayon Mousavi, S.; Graef, W.; Mihailova, D.; Kozák, T.; Bogaerts, A.; van Dijk, J. A Comprehensive Chemical Model for the Splitting of CO_2 in Non-Equilibrium Plasmas. *Plasma Processes Polym.* **2017**, *14*, 1600155.

(45) Aerts, R.; Martens, T.; Bogaerts, A. Influence of Vibrational States on CO_2 Splitting by Dielectric Barrier Discharges. *J. Phys. Chem. C* **2012**, *116*, 23257–23273.

(46) Blauer, J. A.; Gilmore, G. R. *A Survey of Vibrational Relaxation Rate Data for Processes Important to CO_2-N_2-H_2O Infrared Plume Radiation*; Technical Report AFRPL-TR-73-57, 1973.

(47) Pitchford, L. C.; Alves, L. L.; Bartschat, K.; Biagi, S. F.; Bordage, M.-C.; Bray, I.; Brion, C. E.; Brunger, M. J.; Campbell, L.; Chachereau, A. et al. LXCat: an Open-Access, Web-Based Platform for Data Needed for Modeling Low Temperature Plasmas. *Plasma Processes Polym.* **2017**, *14*, 1600098.

(48) Schwartz, R. N.; Slawsky, Z. I.; Herzfeld, K. F. Calculation of Vibrational Relaxation Times in Gases. *J. Chem. Phys.* **1952**, *20*, 1591.

(49) Grofulović, M.; Alves, L. L.; Guerra, V. Electron-Neutral Scattering Cross Sections for CO_2: a Complete and Consistent Set and an Assessment of Dissociation. *J. Phys. D: Appl. Phys.* **2016**, *49*, 395207.

(50) Itikawa, Y. Cross Sections for Electron Collisions with Carbon Monoxide. *J. Phys. Chem. Ref. Data* **2015**, *44*, 013105.

(51) Klarenaar, B. L. M.; Engeln, R.; van den Bekerom, D. C. M.; van de Sanden, M. C. M.; Morillo-Candas, A. S.; Guaitella, O. Time Evolution of Vibrational Temperatures in a CO_2 Glow Discharge Measured with Infrared Absorption Spectroscopy. *Plasma Sources Sci. Technol.* **2017**, *26*, 115008.

Graphical TOC Entry

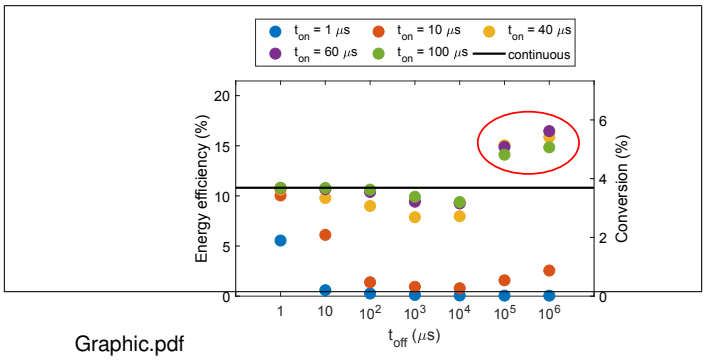

Graphic.pdf

Supporting Information: Improving the Energy Efficiency of CO_2 Conversion in Non-equilibrium Plasmas Through Pulsing

Vincent Vermeiren and Annemie Bogaerts*

Department of Chemistry, Research group PLASMANT, University of Antwerp, Universiteitsplein 1, 2610 Antwerp, Belgium

E-mail: annemie.bogaerts@uantwerpen.be

1 List of Chemical Reactions Included in the Model

Table S1: Electron impact reactions calculated with cross sections, using the calculated EEDF, as explained in section 2.3 of the main paper, as well as the references where the data are adopted from.

No.	Reaction	Ref	Note*
(X1)[a]	$e^- + CO_2 \rightarrow 2e^- + CO_2^+$	S1	
(X2)[b]	$e^- + CO_2 \rightarrow 2e^- + O + CO^+$	S1	
(X3)[b]	$e^- + CO_2 \rightarrow O^- + CO$	S1	
(X4)[b]	$e^- + CO_2 \rightarrow e^- + O + CO$	S1	
(X5)[a]	$e^- + CO_2 \rightarrow e^- + CO_2[e_1]$	S1	
(X6)[c]	$e^- + CO_2 \leftrightarrow e^- + CO[v_i]$	S1	i=a,b,c,d
(X7)[c]	$e^- + CO_2[v_i] \leftrightarrow e^- + CO_2[v_j]$	S1	i,j=0-21
(X8)[b]	$e^- + CO \rightarrow 2e^- + CO^+$	S2	
(X9)[b]	$e^- + CO \rightarrow C + O^-$	S3	
(X9bis)[b]	$e^- + CO \rightarrow e^- + C + O$	S4	
(X10)[a]	$e^- + CO \rightarrow e^- + CO[e_x]$	S4	x=1-4
(X11)[c]	$e^- + CO \rightarrow e^- + CO[v_i]$	S4	i=1-10
(X12)[b]	$e^- + O_2 \rightarrow e^- + O + O$	S5	
(X12M)[a]	$e^- + O_2 + M \rightarrow e^- + O_2^- + M$	S5	
(X13)[b]	$e^- + O_2 \rightarrow O + O^-$	S5	
(X14)[c]	$e^- + O_2 \leftrightarrow e^- + O_2[v_i]$	S5	i=1,2,3
(X15)[a]	$e^- + O_2 \leftrightarrow e^- + O_2[e_x]$	S5	x=1,2

a) Same cross section also used for $CO_2 v_i$ (i = the various vibrationally excited levels)
b) Cross section also used for $CO_2 v_i$, modified by lowering the energy threshold by the energy of the excited state of $CO_2 v_i$
c) Cross section for the various levels (i,j) scaled and shifted using Fridman's approximation from the $(0 \rightarrow 1)$ cross-section
* v_0 is ground state

Table S2: Electron impact reactions using analytical expressions for the rate coefficients, given in m^3/s and m^6/s, for two-body and three-body reactions, respectively, as well as the references where the data are adopted from. T_g and T_e are given in K and eV, respectively.

No.	Reaction	Rate coefficient	Reference
(E1a)	$e^- + CO_2^+ \rightarrow CO(v_1) + O$	$1 \times 10^{-11} T_e^{-0.5} T_g^{-1}$	S6,S7
(E1b)	$e^- + CO_2^+ \rightarrow C + O_2$	$1 \times 10^{-11} T_e^{-0.5} T_g^{-1}$	S8
(E2)[a]	$e^- + CO_4^+ \rightarrow CO_2 + O_2$	$1.61 \times 10^{-13} T_e^{-0.5}$	S8
(E3)	$e^- + CO^+ \rightarrow C + O$	$3.46 \times 10^{-14} T_e^{-0.48}$	S9,S10
(E4)[a]	$e^- + O + M \rightarrow O^- + M$	1×10^{-43}	S7

[a] The primary source was not accessible

Table S3: Ion-ion and ion-neutral reactions, as well as the references where the data are adopted from. The rate coefficients are given in m^3/s and m^6/s, for two-body and three-body reactions, respectively. T_g is given in K.

No.	Reaction	Rate coefficient	Reference
(I1)	$CO_2 + CO^+ \rightarrow CO_2^+ + CO$	1.0×10^{-15}	S11,S12
(I2a)[b]	$CO_2 + O^- + CO_2 \rightarrow CO_3^- + CO_2$	1.5×10^{-40}	S11,S13
(I2b)[b]	$CO_2 + O^- + CO \rightarrow CO_3^- + CO$	1.5×10^{-40}	S11,S13
(I2c)	$CO_2 + O^- + O_2 \rightarrow CO_3^- + O_2$	3.1×10^{-40}	S11,S13
(I3)	$CO_2 + O_2^- + M \rightarrow CO_4^- + M$	4.7×10^{-41}	S11,S13
(I4)	$CO + O^- \rightarrow CO_2 + e$	5.5×10^{-16}	S11,S14
(I5)	$CO + CO_3^- \rightarrow 2CO_2 + e$	5×10^{-19}	S15
(I6)[a]	$CO_3^- + CO_2^+ \rightarrow 2CO_2 v_b + O$	5×10^{-13}	S7
(I7)[a]	$CO_4^- + CO_2^+ \rightarrow 2CO_2 v_b + O_2$	5×10^{-13}	S7
(I8)[a]	$O_2^- + CO_2^+ \rightarrow CO_2 v_1 + O_2 + O$	6×10^{-13}	S7
(I9)	$CO_3^- + O \rightarrow CO_2 + O_2^-$	8×10^{-17}	S16
(I10a)[a]	$CO_4^- + O \rightarrow CO_3^- + O_2$	1.12×10^{-16}	S11
(I10b)[a]	$CO_4^- + O \rightarrow CO_2 + O_2 + O^-$	1.4×10^{-17}	S11
(I11)	$O + O^- \rightarrow O_2 + e$	2.3×10^{-16}	S17
(I12)[a]	$O + O_2^- \rightarrow O_2 + O^-$	1.5×10^{-16}	S11
(I13)	$O_2^- + M \rightarrow O_2 + M + e$	$2.7 \times 10^{-16} (\frac{T_g}{300})^{0.5} exp(-5590/T_g)$	S18,S19
(I14)[c]	$O^- + M \rightarrow O + M + e$	$2.3 \times 10^{-15} exp(-26000/T_g)$	S19–S21

[a] The primary source was not accessible

[b] The rate coefficient of $CO_2 + O^- + He \rightarrow CO_3^- + He$ was used, due to the lack of further information.

[c] For usual values of gas temperature, i.e. $T_g \ll 26000$ K, the rate coefficient is very low, as pointed out by Gudmundsson.[S22]

Table S4: Neutral-neutral reactions, as well as the references where the data are adopted from. The rate coefficients are given in m^3/s and m^6/s, for two-body and three-body reactions, respectively. T_g is given in K. The α parameter determines the effectiveness of lowering the activation energy for reactions involving vibrationally excited levels of the molecules (see details in S23,S24).

No.	Reaction	Rate coefficient	α	References
(N1)	$CO_2 + M \rightarrow CO + O + M$	$6.06 \times 10^{-16} exp(-52525/T_g)$	0.82	S25
(N2)	$CO_2 + O \rightarrow CO + O_2$	$2.8 \times 10^{-17} exp(-16400/T_g)$	0.57	S26
(N3)	$CO_2 + C \rightarrow 2CO$	$< 10^{-21}$	n.a.	S27
(N4)[a]	$CO + O + M \rightarrow CO_2 + M$	$8.3 \times 10^{-46} exp(-1510/T_g)$	0.0	S28,S29
(N5)	$O_2 + CO \rightarrow CO_2 + O$	$4.2 \times 10^{-18} exp(-24000/T_g)$	0.5	S29
(N6)	$O_2 + C \rightarrow CO + O$	$1.99 \times 10^{-16} exp(-2010/T_g)$	0.0	S30
(N7)	$O + C + M \rightarrow CO + M$	$2.14 \times 10^{-41} (\frac{T_g}{300})^{-3.08} exp(-2144/T_g)$	n.a.	S29,S31
(N8)	$O + O + M \rightarrow O_2 + M$	$5.2 \times 10^{-47} exp(900/T_g)$	n.a.	S29,S31
(N9)	$O_2 + M \rightarrow O + O + M$	$3.0 \times 10^{-12} \frac{1}{T_g} exp(-59380/T_g)$	0.0	S29,S31

[a] Multiply by 7, 3 or 12 for M= CO_2, CO or O_2 respectively.

Table S5: Neutral reactions between vibrationally excited molecules, as well as the references where the data are adopted from. The rate coefficients are given in m^3/s and m^6/s, for two-body and three-body reactions, respectively. T_g is given in K.

No.	Reaction	Rate coefficient	References
(V1)	$CO_2 v_a + M \rightarrow CO_2 + M$	$7.14 \times 10^{-15}\, exp(-177\, T_g^{-1/3} + 451\, T_g^{-2/3})$	S32–S34
(V2a)	$CO_2 v_1 + M \rightarrow CO_2 v_a + M$	$4.25 \times 10^{-7}\, exp(-407\, T_g^{-1/3} + 824\, T_g^{-2/3})$	S34–S36
(V2b)	$CO_2 v_1 + M \rightarrow CO_2 v_b + M$	$8.57 \times 10^{-7}\, exp(-404\, T_g^{-1/3} + 1096\, T_g^{-2/3})$	S34–S36
(V2c)	$CO_2 v_1 + M \rightarrow CO_2 v_c + M$	$1.43 \times 10^{-7}\, exp(-252\, T_g^{-1/3} + 685\, T_g^{-2/3})$	S34–S36
(V3)	$CO v_1 + M \rightarrow CO + M$	$1.0 \times 10^{-18}\, T_g\, exp(-150.7\, T_g^{-1/3})$	S37
(V4)	$O_2 v_1 + M \rightarrow O_2 + M$	$1.3 \times 10^{-14}\, exp(-158.7\, T_g^{-1/3})$	S33,S34
(V5)	$CO_2 v_1 + CO_2 \rightarrow CO_2 v_a + CO_2 v_b$	$1.06 \times 10^{-11}\, exp(-242\, T_g^{-1/3} + 633\, T_g^{-2/3})$	S34–S36
(V6)	$CO_2 v_1 + CO_2 \rightarrow CO_2 + CO_2 v_1$	$1.32 \times 10^{-18}\, (\frac{T_g}{300})^{0.5} \frac{250}{T_g}$	S38,S39
(V7)	$CO v_1 + CO \rightarrow CO + CO v_1$	$3.4 \times 10^{-16} (\frac{T_g}{300})^{0.5}\, (1.64 \times 10^{-6}\, T_g + \frac{1.61}{T_g})$	S40,S41
(V8)	$CO_2 v_1 + CO \rightarrow CO_2 + CO v_1$	$4.8 \times 10^{-12}\, exp(-153\, T_g^{-1/3})$	S34,S35

2 Average Temperature Gains and Losses by Plasma Pulsing

Figure 5 in the main paper shows the total vibrational and gas temperature gains and losses between the pulses for different plasma pulse and interpulse times. Here we show the temperature gains and losses, averaged over all pulses, for exactly the same plasma pulse and interpulse times. This gives additional information about the actual temperature values. It is clear that the average gas temperature losses rise with increasing interpulse time.

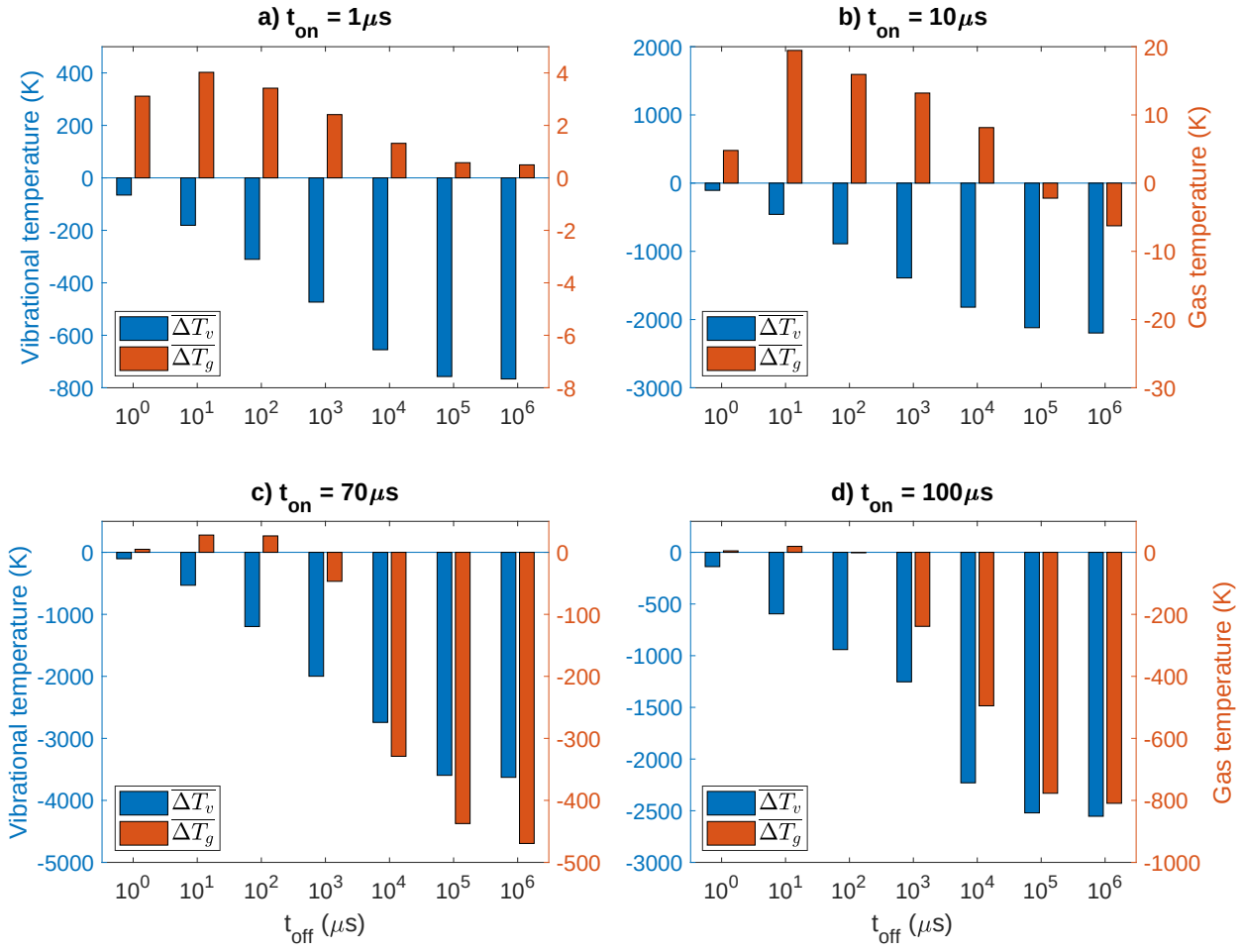

Figure S1: Average vibrational and gas temperature gains and losses between the pulses, for different plasma pulse and interpulse times.

3 Temporal Evolution of the Gas Temperature

In figure S2, we show the evolution of the gas temperature from the initial time t_0 until the plasma end time t_{end} (when the total fixed SEI of 1 eV/molec is reached), for four different plasma pulse times (t_{on} = 1, 10, 70, and 100 μs)and five different interpulse times (t_{off} = 10 μs, 100 μs, 1 ms, 10 ms, 1 s). For comparison, we also plot the gas temperature evolution for the continuous plasma with the same SEI. The x-axis represents the time from the start of the first pulse to the end of the last pulse. However, because the total time is different for different plasma pulse and interpulse times, to reach the same SEI, the reader should not compare different points on the x-axis, since they can represent different total times.

For all of the plasma pulse times, a longer interpulse time yields a lower maximum gas temperature, since there is more cooling. Moreover, the maximum gas temperature is lower than in the continuous plasma for all plasma pulse and interpulse times. At t_{off} = 1 s, the gas temperature completely drops to room temperature. With increasing plasma pulse times, it can be seen that the gas maximum for a given interpulse time increases.

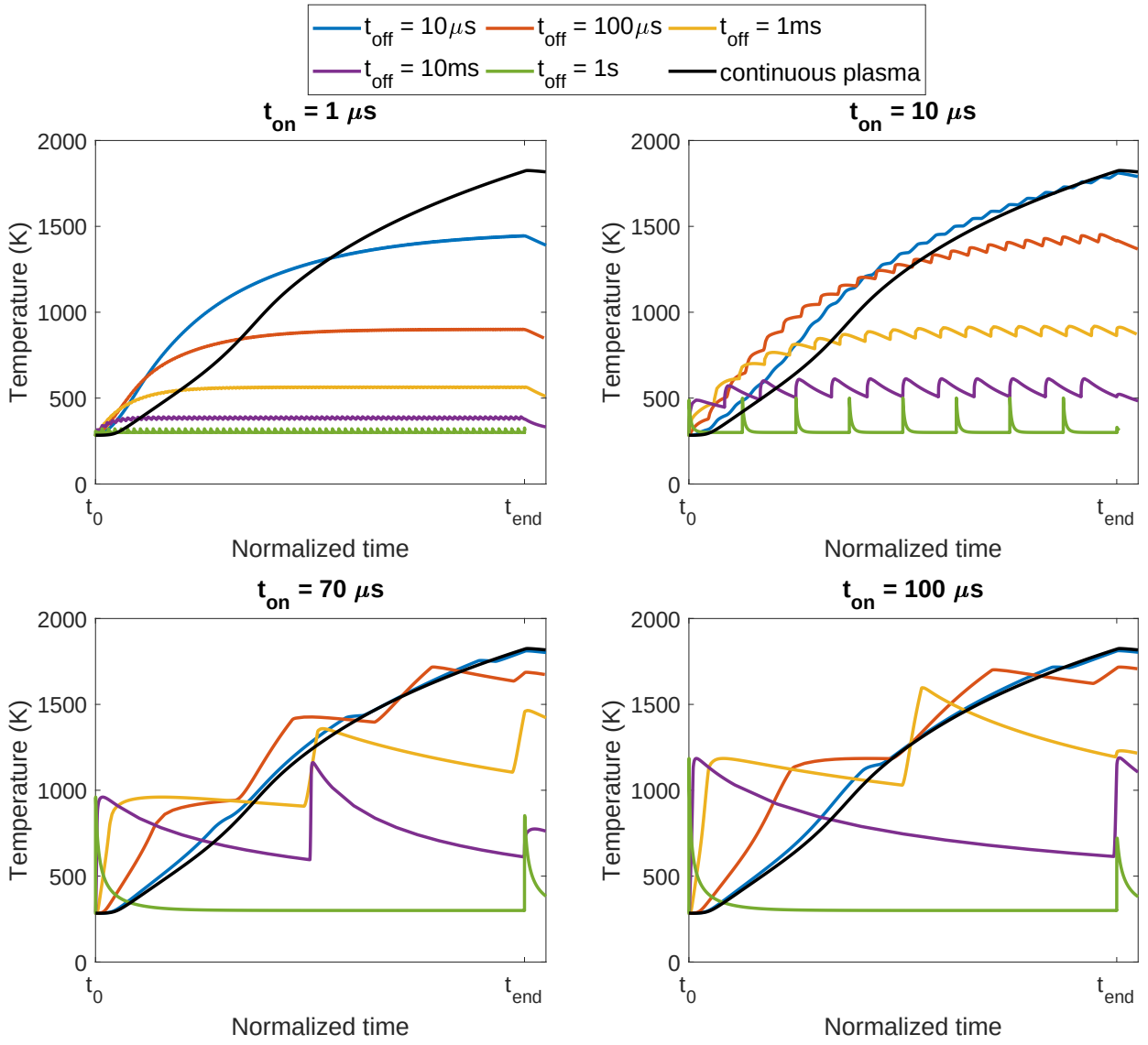

Figure S2: Time-evolution of the gas temperature between the start of the first pulse and the end of the last pulse, for different plasma pulse times and interpulse times. t_{end} is defined by the time when the total fixed SEI of 1 eV/molec is reached. For comparison, the gas temperature in the continuous plasma, for the same SEI, is also plotted (black curves).

4 Average Vibrational and Gas Temperature During the Pulses

Figure S3 illustrates the average vibrational and gas temperature during the pulses (i.e., averaged over all plasma pulse times), for different plasma pulse and interpulse times, as well as the corresponding values in the continuous plasma, for comparison. For short plasma pulse

times, the vibrational temperature is always lower than in the continuous plasma. Indeed, the pulses are too short to reach a maximum vibrational temperature. For longer plasma pulse times, the vibrational temperature becomes higher than in the continuous plasma at interpulse times above 1 ms, because of the enhanced cooling, causing less VT relaxation. In all cases, the average gas temperature is comparable to a continuous plasma for short interpulse times (below 1 ms), and drops with increasing interpulse time. This is consistent with figure S2. Note that while for both $t_{on} = 70$ μs and $t_{on} = 100$ μs, the average vibrational temperature at $t_{off} = 10$ ms lies above the continuous plasma, these pulse conditions do not show an increased energy efficiency. Indeed, while the vibrational-translational non-equilibrium is enhanced by the plasma cooling, leading to a higher vibrational temperature, the enhancement is not sufficient to create a fast overpopulation of the vibrational levels (as seen in figure 8 of the main paper, and figure S5 below).

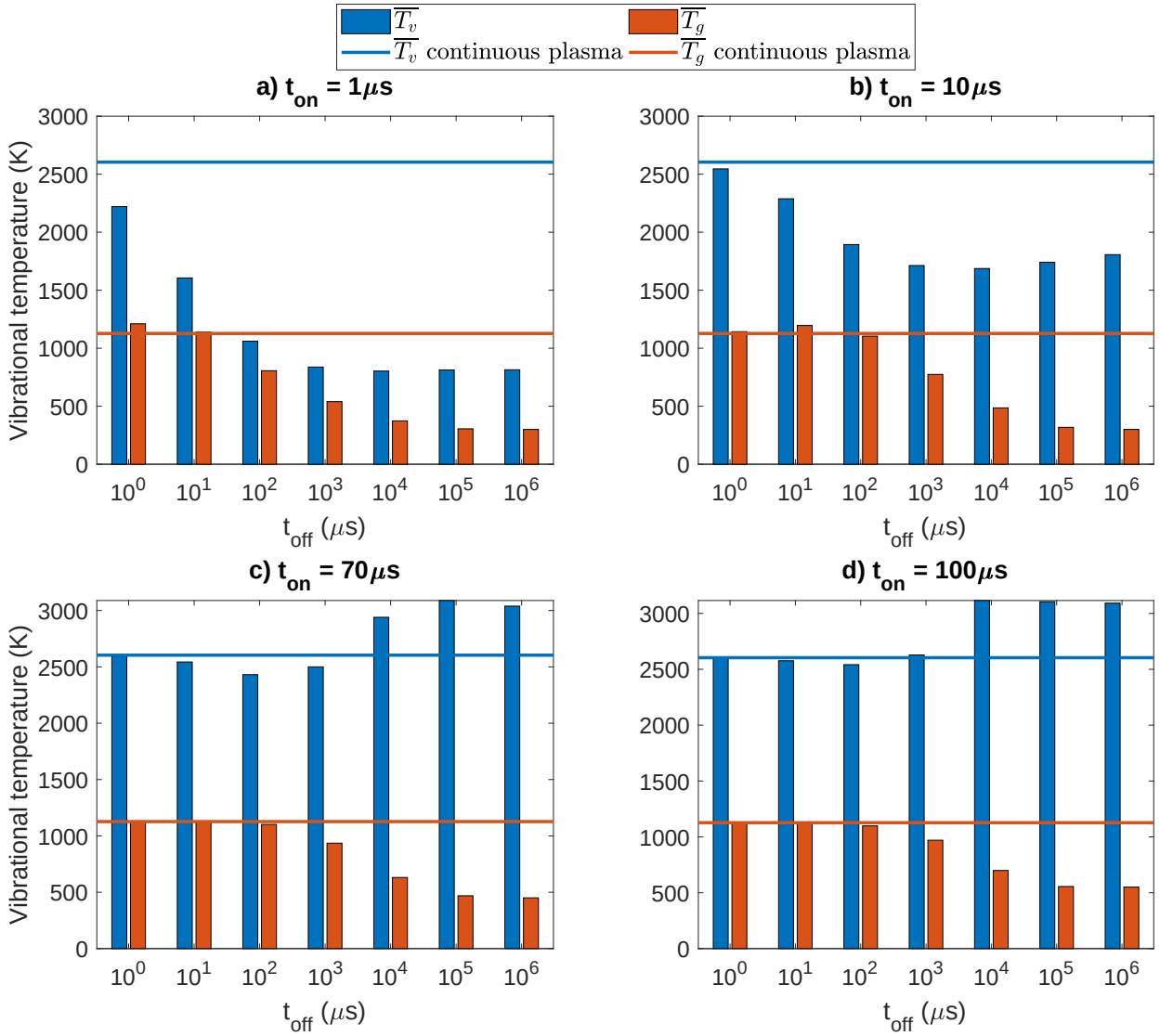

Figure S3: Average vibrational and gas temperature in the plasma pulses for different plasma pulse and interpulse times. The horizontal lines correspond to the continuous plasma.

5 VDF Halfway the Plasma

Figure S4 illustrates the VDFs halfway of the plasma, i.e., when half of the SEI (thus 0.5 eV/molec) is deposited. For $t_{on} = 70$ μs and $t_{on} = 100$ μs, this happens in the first pulse, so we only show the VDFs for shorter plasma pulses, i.e., $t_{on} = 1$ μs and $t_{on} = 10$ μs. We also compare with the VDF in the continuous plasma, and with the Boltzmann plots at the corresponding gas temperatures. For $t_{on} = 1$ μs (panel a), the VDFs are always lower than in the continuous plasma, and they are most populated for short interpulse times, when there

is limited time for relaxation. At longer interpulse times, the VDF completely relaxes in between the pulses, and the pulse time is too short to reach significant overpopulation of the vibrational levels. At $t_{on} = 10$ μs, the VDF coincides with the continuous plasma at short interpulse times, but it is depleted for longer interpulse times. However, due to the low gas temperature at $t_{off} = 1$ s, the characteristic time scales of the VV relaxation is low, while that of the VT relaxation is high, resulting again in a fast and pronounced overpopulation of the higher vibrational levels, so the VDF becomes again very similar to that of a continuous plasma.

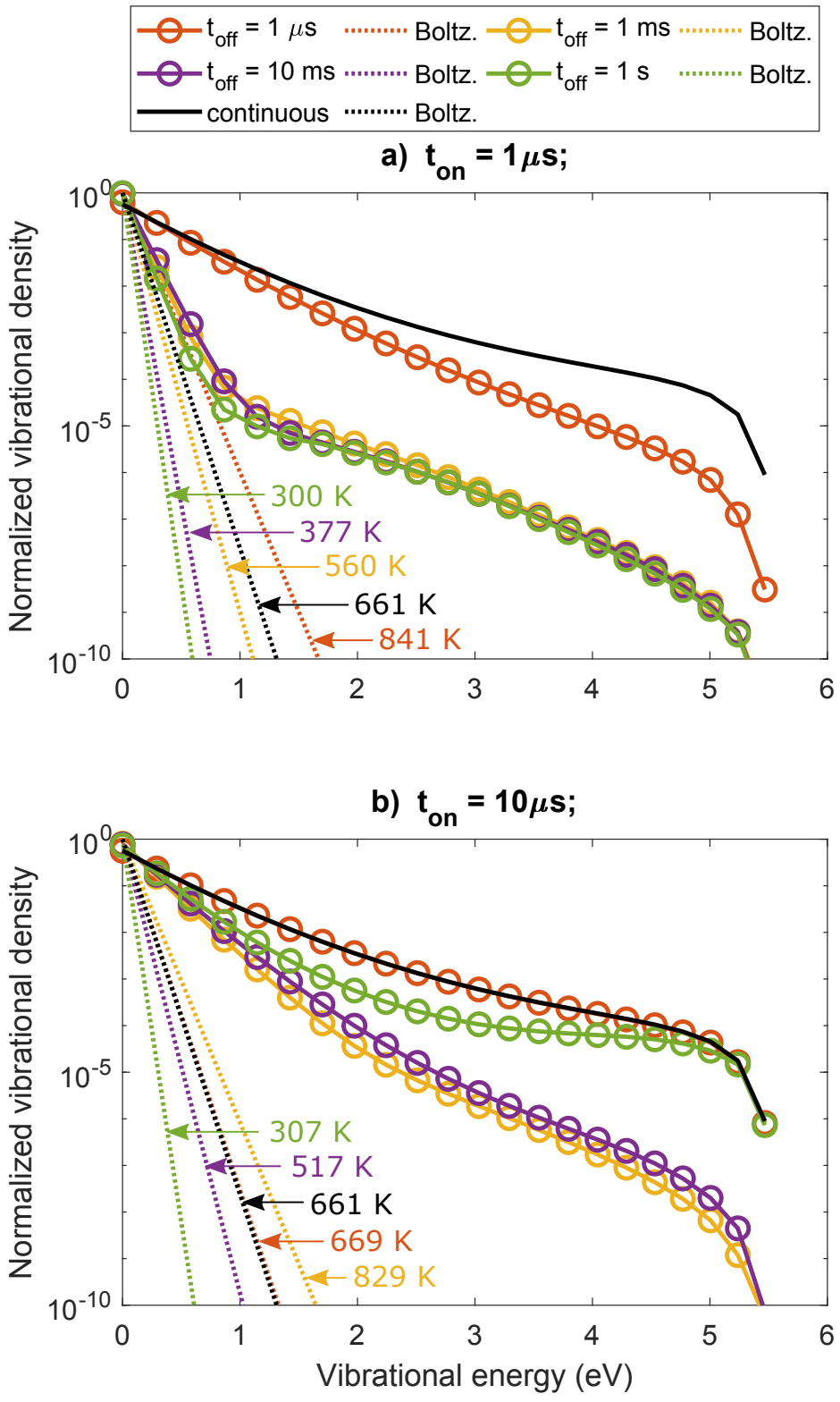

Figure S4: VDFs halfway the plasma, i.e., when half of the SEI is deposited (0.5 eV/molec), for $t_{on} = 1$ μs (a, top panel), and for $t_{on} = 10$ μs (b, bottom panel), and for four different interpulse times. The VDF in the continuous plasma is also plotted (black curve), as well as the Boltzmann plots for each case at the corresponding gas temperatures.

6 VDF at the End of the Plasma

In figure S5, we plot the VDFs at the end of the plasma, for t_{on} = 10 μs and t_{on} = 100 μs. They should be compared with the VDFs for t_{on} = 1 and 70 μs, plotted in figure 9 of the main paper.

For t_{on} = 10 μs and t_{on} = 100 μs, the VDFs at the end of the plasma, for different interpulse times look very similar to the VDFs for 70 μs. The VDF at the end of the plasma coincides with the one of the continuous plasma for short interpulse times (1 μs to 1 ms), but it reaches a higher population for longer interpulse times, similar to t_{on} = 70 μs (see figure 9 of the main paper). However, while both plasma pulse time show a large overpopulation of the VDF at t_{off} = 1 s, the energy efficiency with respect to t_{on} = 70 μs remains lower. Indeed, for t_{on} = 10 μs, the short plasma pulse time enhances the vibrational temperature loss due to pulsing (see figure 6 in the main paper). Also, while the overpopulation at the end of the pulse is high, the overpopulation does not last long enough for vibrational induced dissociation. For t_{on}=100 μs, there are two pulses to reach the SEI of 1 eV/molec at t_{off} = 1 s. However, during a significant portion of the first pulse, the VDF was thermalized, so our model predicts lower energy efficiencies for these conditions than for t_{on} = 70 μs (see figure 1 in the main paper).

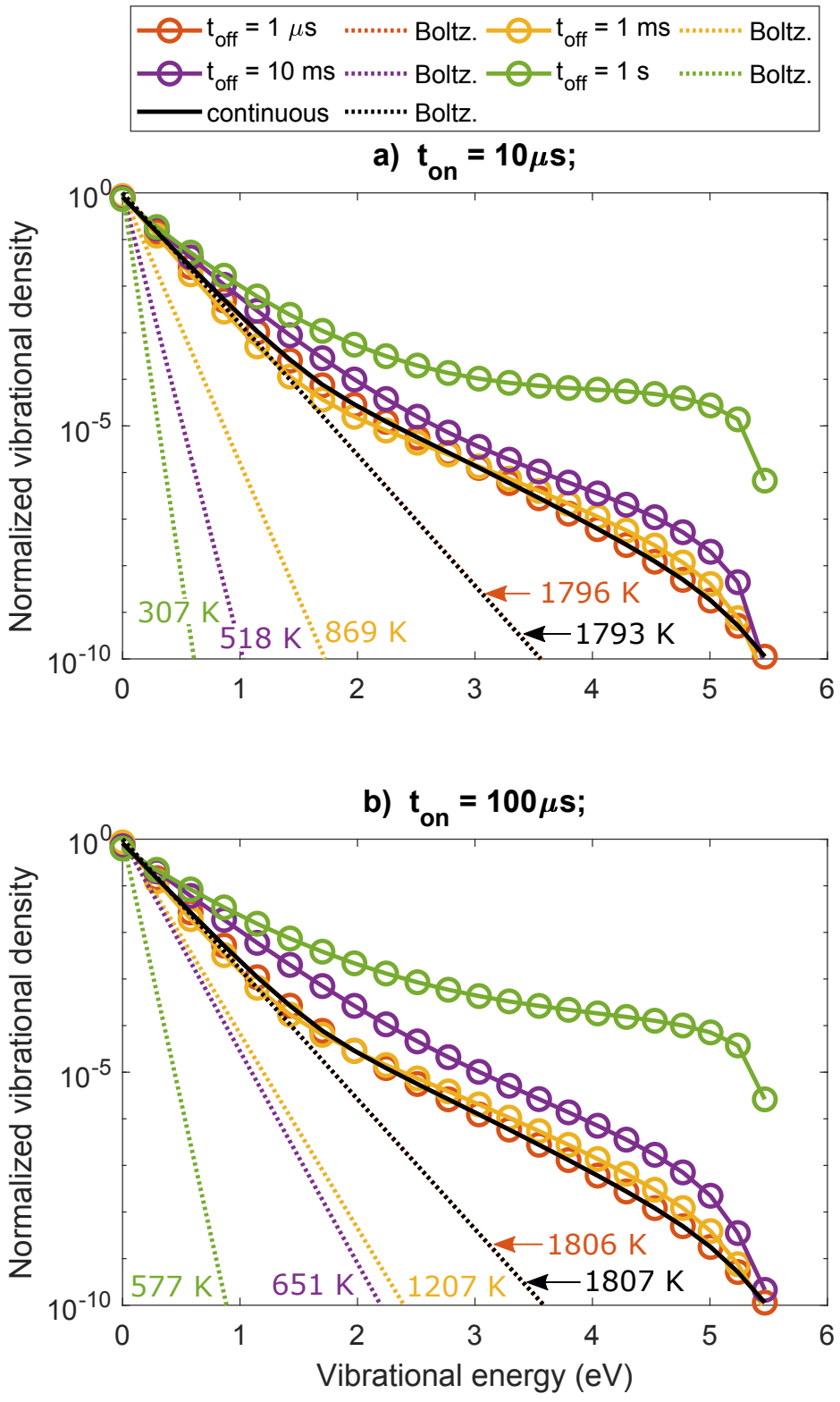

Figure S5: VDFs at the end of the plasma, for $t_{on} = 1$ μs (a, top panel), and $t_{on} = 100$ μs (b, bottom panel) for four different interpulse times. The VDF in the continuous plasma is also plotted (black curve), as well as the Boltzmann plots for each case at the corresponding gas temperatures.

7 Time-evolution of the Vibrational and Gas Temperature in a Continuous Plasma for Different Ionization Degrees and Reduced Electric Fields

Figures S6-S8 show the time-evolution of the vibrational and gas temperature in a continuous plasma, for different ionization degrees, and for reduced electric fields of 50 Td, 100 Td and 150 Td, respectively. The end time is different in each case, as it is defined by the time when the total fixed SEI of 1 eV/molec is reached. At low ionization degrees, the vibrational temperature reaches a maximum value early in time, but this maximum shifts to later times upon higher ionization degree. This is correlated with the lower characteristic time scale of electron impact vibrational excitation with higher ionization degree, as was shown in figure 2 of the main paper. At an ionization degree of 5×10^{-6} and higher, the maximum value is reached close to or at the end of the plasma (i.e., when the SEI of 1 eV/molec is reached). For these conditions, pulsing will not increase the energy efficiency, because the loss of vibrational energy between the pulses will not be compensated by a higher vibrational temperature. This is true for a reduced electric field of 50 and 100 Td (figures S6 and S7). At 150 Td, this is already the case for an ionization degree of 5×10^{-7} (figure S8).

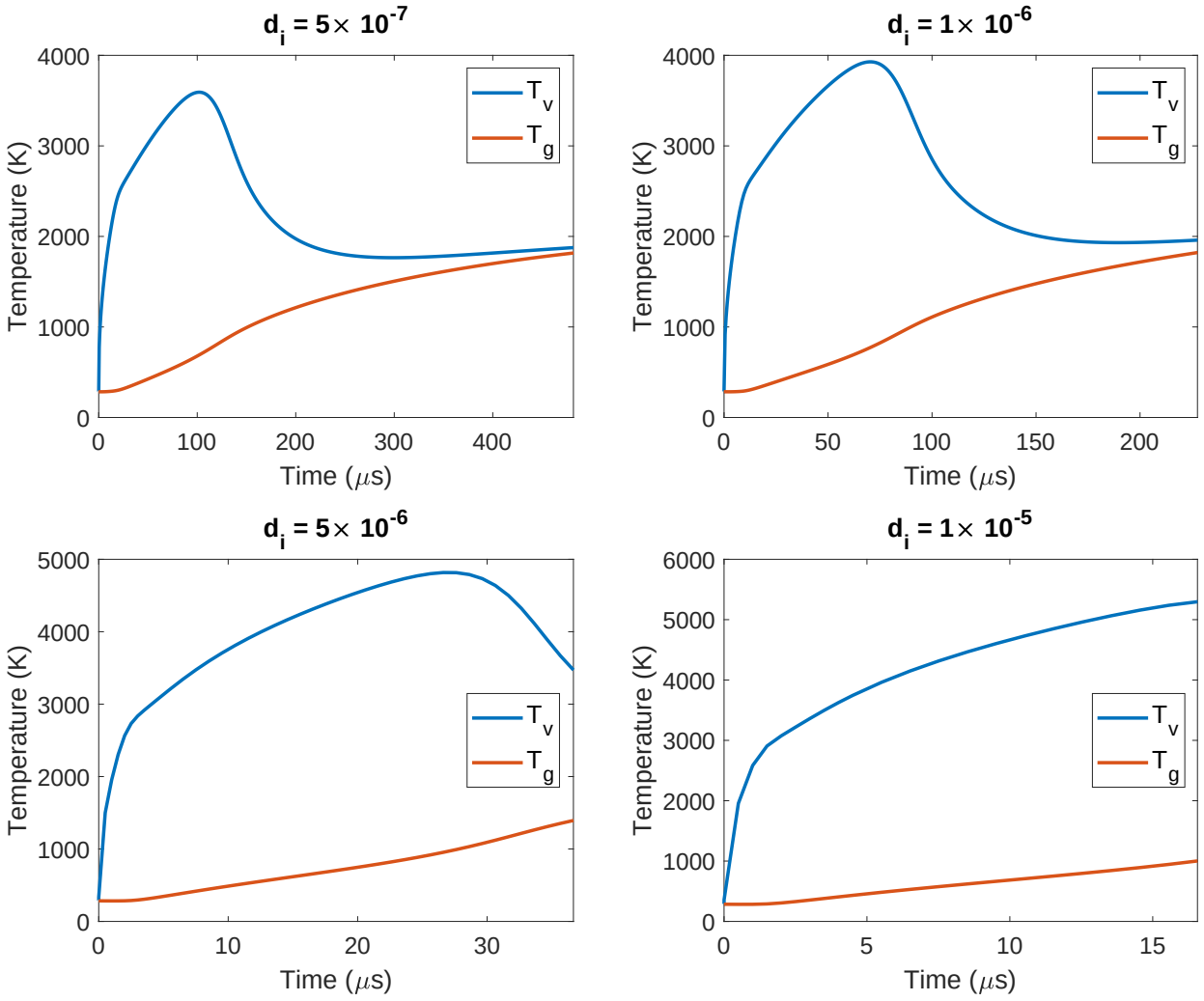

Figure S6: Time-evolution of the vibrational and gas temperature in a continuous plasma for different ionization degrees, and a reduced electric field of 50 Td.

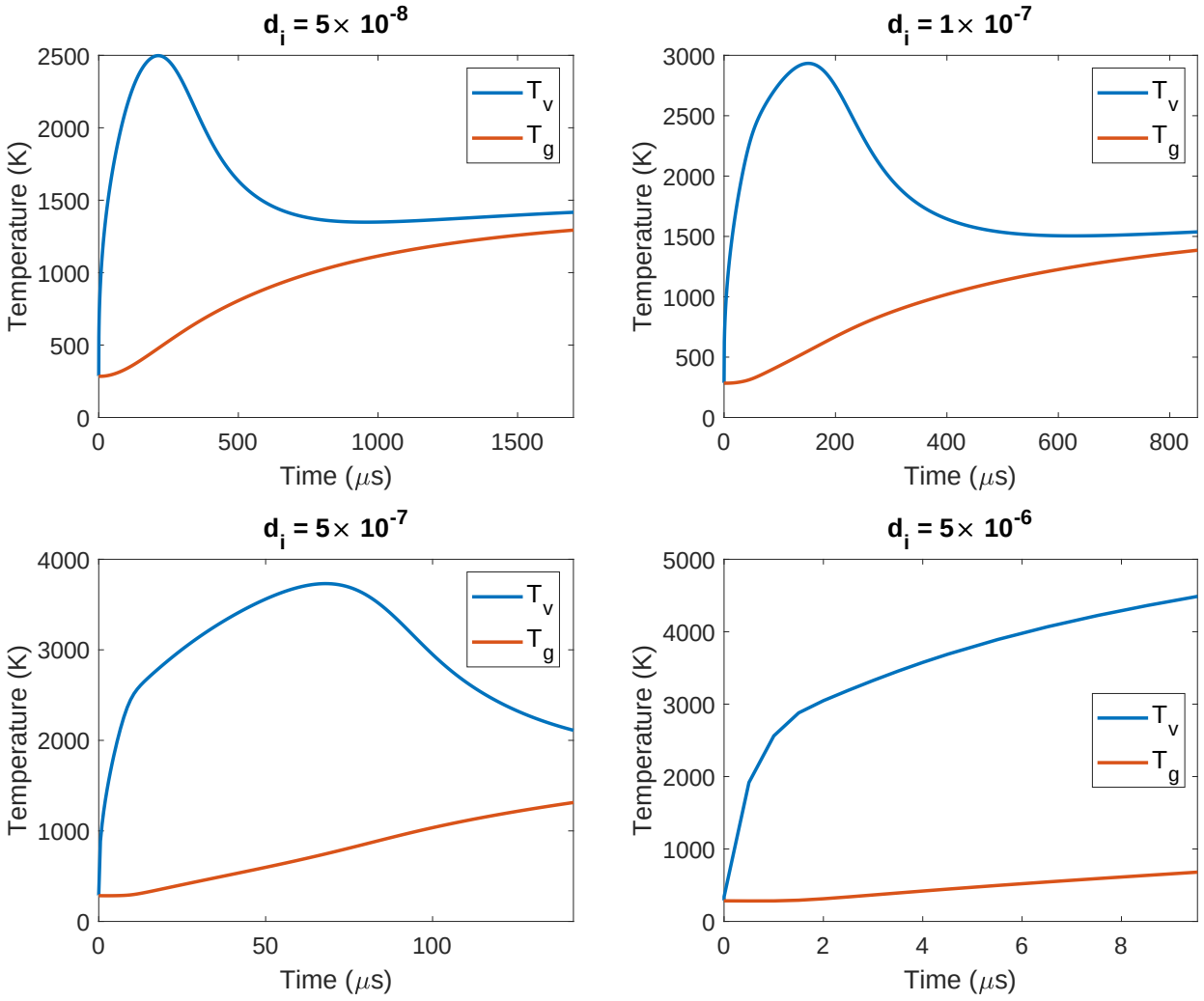

Figure S7: Time-evolution of the vibrational and gas temperature in a continuous plasma for different ionization degrees, and a reduced electric field of 100 Td.

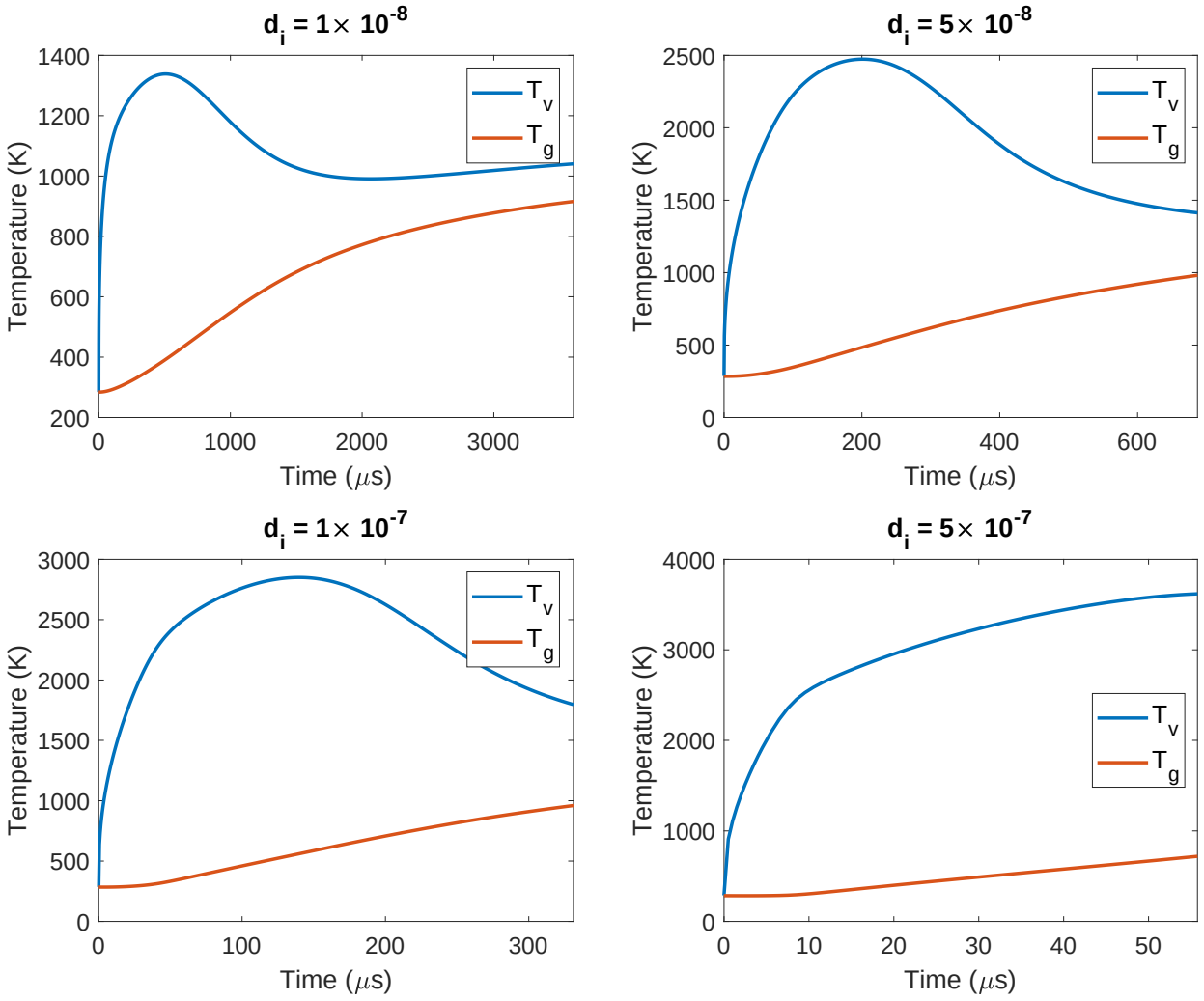

Figure S8: Time-evolution of the vibrational and gas temperature in a continuous plasma for different ionization degrees, and a reduced electric field of 150 Td.

8 Dissociation Mechanisms for Different Reduced Electric Fields and an Ionization Degree of 10^{-7}

In figures 11 and 12 of the main paper, it was shown that at low ionization degrees, plasma pulsing did not enhance the energy efficiency of the continuous plasma, while we showed above that the vibrational temperature did thermalize at the end of the continuous plasma (see e.g. $d_i = 10^{-7}$ in figures S6-S8). In this section, we will explain this by examining the dissociation mechanisms for pulsed plasmas with an ionization degree of 10^{-7}, at reduced electric fields of 50 Td, 100 Td, and 150 Td (figures S9- S11). In figure S9, the conversion by the three main dissociation mechanisms is shown for different plasma pulse times, at an interpulse time of 1 s, a reduced electric field of 50 Td, and an ionization degree of 10^{-7}. The corresponding values for the continuous plasma are indicated with horizontal lines in the same color. At short plasma pulse times, only electron impact dissociation plays a role, and vibrational induced dissociation is negligible. Indeed, the VDF does not have enough time to get fully populated. At plasma pulse times of 200 μs and above, vibrational induced dissociation upon collision with a molecule M shows an increased performance with respect to the continuous plasma, but it is not the most important dissociation process. Indeed, electron impact dissociation is still more important. Nevertheless, the conversion due to electron impact dissociation is severely reduced upon pulsing, as illustrated in figure S9. This reduction is enough to counter the increase in vibrational induced dissociation upon collision with a molecule M, and will therefore lead to a lower total conversion and energy efficiency. Upon increasing reduced electric field, electron impact dissociation becomes more important,[S42] so similar trends are observed in figures S10 and S11 for 100 Td and 150 Td, respectively, again at an ionization degree of 10^{-7}, where also the rise in vibrational induced dissociation is countered by a drop in electron impact dissociation.

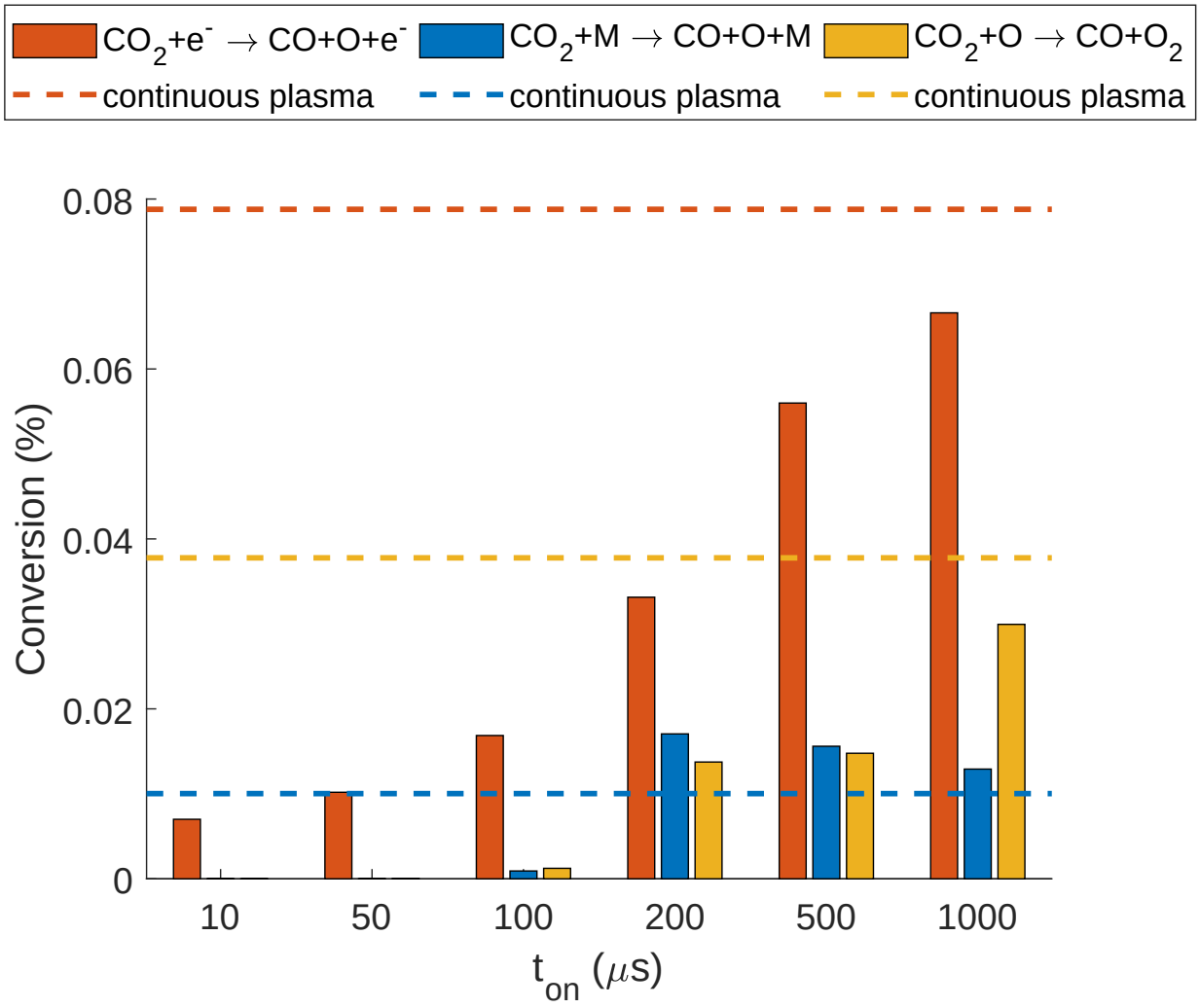

Figure S9: CO_2 conversion by the three main dissociation reactions: electron impact dissociation (red), dissociation upon collision with a molecule M (blue) and upon collision with an O atom (yellow), for different plasma pulse times and an interpulse time of 1 s, a reduced electric field of 50 Td and an ionization degree of 10^{-7}. The dashed horizontal lines represent the respective conversions of a continuous plasma at the same SEI.

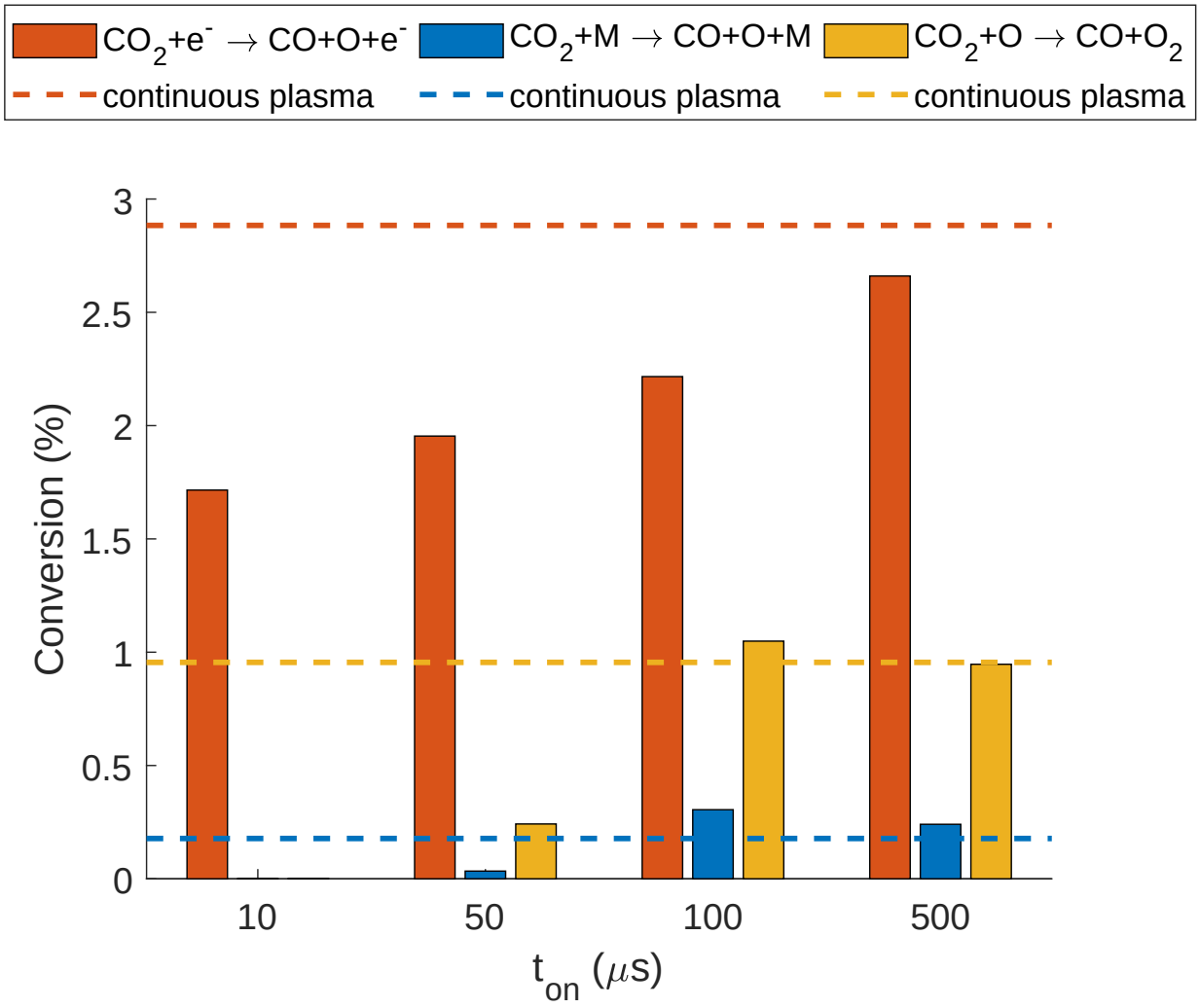

Figure S10: CO_2 conversion by the three main dissociation reactions: electron impact dissociation (red), dissociation upon collision with a molecule M (blue) and upon collision with an O atom (yellow), for different plasma pulse times and an interpulse time of 1 s, a reduced electric field of 100 Td and an ionization degree of 10^{-7}. The dashed horizontal lines represent the respective conversions of a continuous plasma at the same SEI.

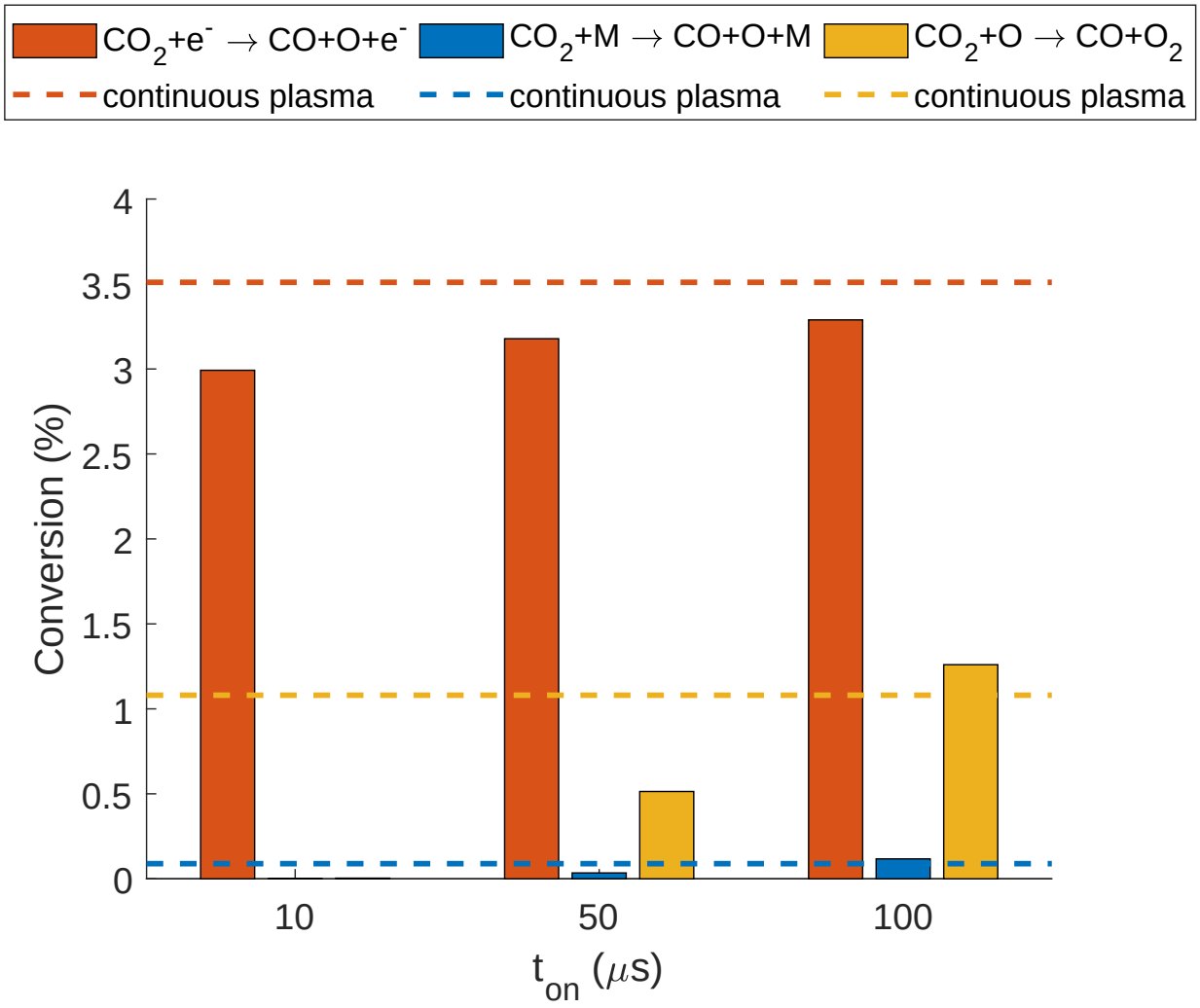

Figure S11: CO_2 conversion by the three main dissociation reactions: electron impact dissociation (red), dissociation upon collision with a molecule M (blue) and upon collision with an O atom (yellow), for different plasma pulse times and an interpulse time of 1 s, a reduced electric field of 150 Td and an ionization degree of 10^{-7}. The dashed horizontal lines represent the respective conversions of a continuous plasma at the same SEI.

9 References

References

(S1) Phelps, A. V. Phelps Database from www.lxcat.net (retrieved September 4, 2014).

(S2) Tian, C.; Vidal, C. R. Cross Sections of the Electron Impact Dissociative Ionization of CO, CH_4 and C_2H_2. *J. Phys. B: At. Mol. Opt. Phys.* **1998**, *31*, 895–909.

(S3) Rapp, D.; Briglia, D. D. Total Cross Sections for Ionization and Attachment in Gases by Electron Impact. II. Negative Ion Formation. *J. Chem. Phys.* **1965**, *43*, 1480–1489.

(S4) Land, J. E. Electron Scattering Cross Sections for Momentum Transfer and Inelastic Excitation in Carbon Monoxide. *J. Appl. Phys.* **1978**, *49*, 5716–5721.

(S5) Lawton, S. A.; Phelps, A. V. Excitation of the $b^1\Sigma_g^+$ State of O_2 by Low Energy Electrons. *J. Chem. Phys.* **1978**, *69*, 1055.

(S6) Weller, C. S.; Biondi, M. A. Measurements of Dissociative Recombination of CO_2^+ Ions with Electrons. *Phys. Rev. Lett.* **1967**, *19*, 59–61.

(S7) Thoenes, J.; Kurzius, S. C. *Plasma Chemistry Processes in the Closed Cycle EDL*; Technical Report DRCPM-HEL-CR-79-11-VOL-1, 1979.

(S8) Beuthe, T. G.; Chang, J.-S. Chemical Kinetic Modelling of Non-Equilibrium Ar-CO_2 Thermal Plasmas. *Jpn. J. Appl. Phys.* **1997**, *36*, 4997–5002.

(S9) Mitchell, J. B. A.; Hus, H. The Dissociative Recombination and Excitation of CO^+. *J. Phys. B: At. Mol. Phys.* **1985**, *18*, 547–555.

(S10) McElroy, D.; Walsh, C.; Markwick, A. J.; Cordiner, M. A.; Smith, K.; Millar, T. J. The UMIST database for astrochemistry 2012. *Astron. Astrophys.* **2013**, *550*, A36.

(S11) Albritton, D. Ion-Neutral Reaction-Rate Constants Measured in Flow Reactors through 1977. *At. Data Nucl. Data Tables* **1978**, *22*, 1–101.

(S12) Adams, N.; Smith, D.; Grief, D. Reactions of H_nCO^+ Ions with Molecules at 300 K. *Int. J. Mass Spectrom. Ion Phys.* **1978**, *26*, 405–415.

(S13) Fehsenfeld, F. C.; Ferguson, E. E. Laboratory Studies of Negative Ion Reactions with Atmospheric Trace Constituents. *J. Chem. Phys.* **1974**, *61*, 3181–3193.

(S14) Mcfarland, M.; Albritton, D. L.; Fehsenfeld, F. C.; Ferguson, E. E.; Schmeltekopf, A. L. Flow-Drift Technique for Ion Mobility and Ion-Molecule Reaction Rate Constant Measurements. III. Negative Ion Reactions of O^- with CO, NO, H_2, and D_2. *J. Chem. Phys.* **1973**, *59*, 6629–6635.

(S15) Price, D.; Moruzzi, J. Negative Ion Molecule Reactions in CO_2 at High Pressures and Temperatures. *Vacuum* **1974**, *24*, 591–593.

(S16) Fehsenfeld, F. C.; Schmeltekopf, A. L.; Schiff, H. I.; Ferguson, E. E. Laboratory Measurements of Negative Ion Reactions of Atmospheric Interest. *Planet. Space Sci.* **1967**, *15*, 373–379.

(S17) Belostotsky, S. G.; Economou, D. J.; Lopaev, D. V.; Rakhimova, T. V. Negative Ion Destruction by $O(^3P)$ Atoms and $O_2(a^1\Delta_g)$ Molecules in an Oxygen Plasma. *Plasma Sources Sci. Technol.* **2005**, *14*, 532–542.

(S18) Pack, J. L.; Phelps, A. V. Electron Attachment and Detachment. II. Mixtures of O_2 and CO_2 and of O_2 and H_2O. *J. Chem. Phys.* **1966**, *45*, 4316–4329.

(S19) Bortner, M. H.; Bourer, T.; Blank, C. A. *Defense Nuclear Agency Reaction Rate Handbook, Second Edition*; Technical report AD 763699, 1972.

(S20) Hasted, J. B.; Smith, R. A. The Detachment of Electrons from Negative Ions. *Proc. R. Soc. London, Ser. A* **1956**, *235*, 349–353.

(S21) Frommhold, L. Über Verzögerte Elektronen in Elektronenlawinen, insbesondere in Sauerstoff und Luft, durch Bildung und Zerfall Negativer Ionen (O^-). *Fortschr. Phys.* **1964**, *12*, 597–642.

(S22) Gudmundsson, J. T. *A Critical Review of the Reaction set for a Low Pressure Oxygen Processing Discharge*; Technical Report RH-17-2004, 2004.

(S23) Fridman, A. *Plasma Chemistry*; Cambridge University Press: New York, USA, 2008.

(S24) Kozák, T.; Bogaerts, A. Splitting of CO_2 by Vibrational Excitation in Non-Equilibrium Plasmas: a Reaction Kinetics Model. *Plasma Sources Sci. Technol.* **2014**, *23*, 045004.

(S25) Burmeister, M.; Roth, P. ARAS Measurements on the Thermal Decomposition of CO_2 Behind Shock Waves. *AIAA Journal* **1990**, *28*, 402–405.

(S26) Clark, T. C.; Garnett, S. H.; Kistiakowsky, G. B. Reaction of Carbon Dioxide with Atomic Oxygen and the Dissociation of Carbon Dioxide in Shock Waves. *J. Chem. Phys.* **1969**, *51*, 2885–2891.

(S27) Husain, D.; Young, A. N. Kinetic Investigation of Ground State Carbon Atoms, $C(2^3P_J)$. *J. Chem. Soc., Faraday Trans. 2* **1975**, *71*, 525.

(S28) Baldwin, R. R.; Jackson, D.; Melvin, A.; Rossiter, B. N. The Second Limit of Hydrogen + Carbon Monoxide + Oxygen Mixtures. *Int. J. Chem. Kinet.* **1972**, *4*, 277–292.

(S29) Tsang, W.; Hampson, R. F. Chemical Kinetic Data Base for Combustion Chemistry. Part I. Methane and Related Compounds. *J. Phys. Chem. Ref. Data* **1986**, *15*, 1087–1279.

(S30) Dean, A. J.; Davidson, D. F.; Hanson, R. K. A Shock Tube Study of Reactions of Carbon Atoms with Hydrogen and Oxygen using Excimer Photolysis of C_3O_2 and

Carbon Atom Atomic Resonance Absorption Spectroscopy. *J. Phys. Chem.* **1991**, *95*, 183–191.

(S31) Baulch, D. L.; Drysdale, D. D.; Duxbury, J.; Grant, S. *Evaluated Kinetic Data for High Temperature Reactions, Volume 3: Homogeneous Gas Phase Reactions of the O_2-O_3 System, the CO-O_2-H_2 System, and of the Sulphur-containing Species*; Butterworth: London, UK, 1976.

(S32) Simpson, C. J. S. M.; Chandler, T. R. D.; Strawson, A. C. Vibrational Relaxation in CO_2 and CO_2–Ar Mixtures Studied Using a Shock Tube and a Laser–Schlieren Technique. *J. Chem. Phys.* **1969**, *51*, 2214–2219.

(S33) Taylor, R. L.; Bitterman, S. Survey of Vibrational Relaxation Data for Processes Important in the CO_2-N_2 Laser System. *Rev. Mod. Phys.* **1969**, *41*, 26–47.

(S34) Blauer, J. A.; Gilmore, G. R. *A Survey of Vibrational Relaxation Rate Data for Processes Important to CO_2-N_2-H_2O Infrared Plume Radiation*; Technical Report AFRPL-TR-73-57, 1973.

(S35) Rosser, W. A.; Wood, A. D.; Gerry, E. T. Deactivation of Vibrationally Excited Carbon Dioxide (ν_3) by Collisions with Carbon Dioxide or with Nitrogen. *J. Chem. Phys.* **1969**, *50*, 4996–5008.

(S36) Herzfeld, K. F. Deactivation of Vibrations by Collision in the Presence of Fermi Resonance. *J. Chem. Phys.* **1967**, *47*, 743–752.

(S37) Capitelli, M.; Ferreira, C. M.; Gordiets, B. F.; Osipov, A. I. *Plasma Kinetics in Atmospheric Gases*; Springer Berlin Heidelberg: Berlin, Germany, 2000.

(S38) Sharma, R. D. Near Resonant Vibrational Energy Transfer among Isotopes of CO_2. *Phys. Rev.* **1969**, *177*, 102–107.

(S39) Kreutz, T. G.; O'Neill, J. A.; Flynn, G. W. Diode Laser Absorption Probe of Vibration-Vibration Energy Transfer in CO_2. *J. Phys. Chem.* **1987**, *91*, 5540–5543.

(S40) DeLeon, R. L.; Rich, J. Vibrational Energy Exchange Rates in Carbon Monoxide. *Chem. Phys.* **1986**, *107*, 283–292.

(S41) Flament, C.; George, T.; Meister, K.; Tufts, J.; Rich, J.; Subramaniam, V.; Martin, J.-P.; Piar, B.; Perrin, M.-Y. Nonequilibrium Vibrational Kinetics of Carbon Monoxide at high Translational Mode Temperatures. *Chem. Phys.* **1992**, *163*, 241–262.

(S42) Berthelot, A.; Bogaerts, A. Pinpointing Energy Losses in CO_2 Plasmas - Effect on CO_2 Conversion. *J. CO_2 Util.* **2018**, *24*, 479–499.